

Differentiable Causal Discovery from Interventional Data

Philippe Brouillard*
Mila, Université de Montréal

Sébastien Lachapelle*
Mila, Université de Montréal

Alexandre Lacoste
Element AI

Simon Lacoste-Julien
Mila, Université de Montréal
Canada CIFAR AI Chair

Alexandre Drouin
Element AI

Abstract

Discovering causal relationships in data is a challenging task that involves solving a combinatorial problem for which the solution is not always identifiable. A new line of work reformulates the combinatorial problem as a continuous constrained optimization one, enabling the use of different powerful optimization techniques. However, methods based on this idea do not yet make use of interventional data, which can significantly alleviate identifiability issues. In this work, we propose a neural network-based method for this task that can leverage interventional data. We illustrate the flexibility of the continuous-constrained framework by taking advantage of expressive neural architectures such as normalizing flows. We show that our approach compares favorably to the state of the art in a variety of settings, including perfect and imperfect interventions for which the targeted nodes may even be unknown.

1 Introduction

The inference of causal relationships is a problem of fundamental interest in science. In all fields of research, experiments are systematically performed with the goal of elucidating the underlying causal dynamics of systems. This quest for causality is motivated by the desire to take actions that induce a controlled change in a system. Achieving this requires to answer questions, such as “what would be the impact on the system if this variable were changed from value x to y ?”, which cannot be answered without causal knowledge [25].

In this work, we address the problem of data-driven causal discovery [13]. Our goal is to design an algorithm that can automatically discover causal relationships from data. More formally, we aim to learn a *causal graphical model* (CGM) [28], which consists of a joint distribution coupled with a directed acyclic graph (DAG), where edges indicate direct causal relationships. Achieving this based on observational data alone is challenging since, under the faithfulness assumption, the true DAG is only identifiable up to a *Markov equivalence class* [38]. Fortunately, identifiability can be improved by considering interventional data, i.e., the outcome of some experiments. In this case, the DAG is identifiable up to an *interventional Markov equivalence class*, which is a subset of the Markov equivalence class [40, 12], and, when observing enough interventions [7, 9], the DAG is exactly identifiable. In practice, it may be possible for domain experts to collect such interventional data, resulting in clear gains in identifiability. For instance, in genomics, recent advances in gene editing technologies have given rise to high-throughput methods for interventional gene expression data [4].

* Equal contribution.

Correspondence to: {philippe.brouillard, sebastien.lachapelle}@umontreal.ca

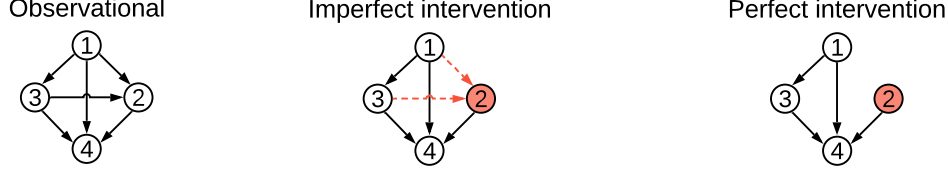


Figure 1: Different intervention types (shown in red). In imperfect interventions, the causal relationships are altered. In perfect interventions, the targeted node is cut out from its parents.

Nevertheless, even with interventional data at hand, finding the right DAG is challenging. The solution space is immense and grows super-exponentially with respect to the number of variables of interest. Recently, Zheng et al. [44] proposed to cast this search problem as a constrained continuous optimization problem, avoiding the computationally intensive search performed by score-based and constrained-based methods [28]. The work of [44] was limited to linear causal relationships, but was quickly extended to nonlinear ones via neural networks [21, 41, 45, 24, 18, 46]. However, such approaches have only been applied to *observational* data under some assumptions (e.g., additive noise models) and cannot make use of interventional data. In this work, we propose a differentiable approach to causal discovery that can make use of *interventional* data to model complex nonlinear causal relationships without making such assumptions.

1.1 Contributions

- We propose the approach Differentiable Causal Discovery with Interventions (DCDI): a general differentiable causal structure learning method that can leverage perfect, imperfect and unknown interventions (Section 3). We propose two instantiations, one of which is a universal density approximator that uses normalizing flows (Section 3.4).
- We prove an identifiability result to support our proposed approach (Theorem 1, Section 3.1).
- We provide an extensive comparison of DCDI to state-of-the-art methods in a wide variety of conditions, including multiple functional forms and types of interventions (Section 4).

2 Background and related work

2.1 Definitions

Causal graphical models. A CGM is defined by a distribution P_X over a random vector $X = (X_1, \dots, X_d)$ and a DAG $\mathcal{G} = (V, E)$. Each node $i \in V = \{1, \dots, d\}$ is associated with a random variable X_i and each edge $(i, j) \in E$ represents a direct causal relation from variable X_i to X_j . The distribution P_X is Markov to the graph \mathcal{G} , which means that the joint distribution can be factorized as such:

$$p(x_1, \dots, x_d) = \prod_{j=1}^d p_j(x_j | x_{\pi_j^{\mathcal{G}}}), \quad (1)$$

where $\pi_j^{\mathcal{G}}$ is the set of parents of the node j in the graph \mathcal{G} , and x_B , for a subset $B \subseteq V$, denotes the entries of the vector x with indices in B . In this work, we assume *causal sufficiency*, i.e., there is no hidden common cause that is causing more than one variable in X [28].

Interventions. In contrast with standard Bayesian Networks, CGMs support interventions. Formally, an intervention on a variable x_j corresponds to replacing its conditional $p_j(x_j | x_{\pi_j^{\mathcal{G}}})$ by a new conditional $\tilde{p}_j(x_j | x_{\pi_j^{\mathcal{G}}})$ in Equation (1), thus modifying the distribution only locally. Interventions can be performed on multiple variables simultaneously and we call *interventional target* the set $I \subseteq V$ of such variables. When considering more than one intervention, we denote the interventional target of the k th intervention by I_k . Throughout this paper, we assume that the observational distribution (the original distribution without interventions) is observed, and denote it by $I_1 := \emptyset$. We define the *interventional family* by $\mathcal{I} := (I_1, \dots, I_K)$, where K is the number of interventions (including the

observational setting). Finally, the k th interventional joint density is

$$p^{(k)}(x_1, \dots, x_d) := \prod_{j \notin I_k} p_j^{(1)}(x_j | x_{\pi_j^{\mathcal{G}}}) \prod_{j \in I_k} p_j^{(k)}(x_j | x_{\pi_j^{\mathcal{G}}}), \quad (2)$$

where the assumption of causal sufficiency is implicit to this definition of interventions.

Type of interventions. The general type of interventions described in (2) are called imperfect (or soft, parametric) [28, 5, 6]. A specific case that is often considered is (stochastic) perfect interventions (or hard, structural) [8, 40, 20] where $p_j^{(k)}(x_j | x_{\pi_j^{\mathcal{G}}}) = p_j^{(k)}(x_j)$ for all $j \in I_k$, thus removing the dependencies with their parents (see Figure 1). Real-world examples of these types of interventions include gene knockout/knockdown in biology. Analogous to a perfect intervention, a gene knockout completely suppresses the expression of one gene and removes dependencies to regulators of gene expression. In contrast, a gene knockdown hinders the expression of one gene without removing dependencies with regulators [47], and is thus an imperfect intervention.

2.2 Causal structure learning

In causal structure learning, the goal is to recover the causal DAG \mathcal{G} using samples from P_X and, when available, from interventional distributions. This problem presents two main challenges: 1) the size of the search space is super-exponential in the number of nodes [3] and 2) the true DAG is not always identifiable (more severe without interventional data). Methods for this task are often divided into three groups: constraint-based, score-based, and hybrid methods. We briefly review these below.

Constraint-based methods typically rely on conditional independence testing to identify edges in \mathcal{G} . The PC algorithm [33] is a classical example that works with observational data. It performs conditional independence tests with a conditioning set that increases at each step of the algorithm and finds an equivalence class that satisfies all independencies. Methods that support interventional data include COMBINE [37] and HEJ [16], which rely on Boolean satisfiability solvers to find a graph that satisfies all constraints. In contrast with our method, these two can account for latent confounders. Another type of constraint-based method exploits the invariance of causal mechanisms across interventional distributions, e.g., ICP [27, 14]. As will later be presented in Section 3, our loss function also accounts for such invariances.

Score-based methods formulate the problem of estimating the ground truth DAG \mathcal{G}^* by optimizing a score function \mathcal{S} over the space of DAGs. The estimated DAG $\hat{\mathcal{G}}$ is given by

$$\hat{\mathcal{G}} \in \arg \max_{\mathcal{G} \in \text{DAG}} \mathcal{S}(\mathcal{G}). \quad (3)$$

A typical choice of score in the purely observational setting is the regularized maximum likelihood score:

$$\mathcal{S}(\mathcal{G}) := \max_{\theta} \mathbb{E}_{X \sim P_X} \log f_{\theta}(X) - \lambda |\mathcal{G}|, \quad (4)$$

where f_{θ} is a density function parameterized by θ , $|\mathcal{G}|$ is the number of edges in \mathcal{G} and λ is a positive scalar.¹ Since the space of DAGs is enormous, these methods often rely on greedy combinatorial search algorithms. A typical example is GIES [12], an adaptation of GES [3] to perfect interventions. In contrast with our method, GIES assumes a *linear* gaussian model and optimizes the Bayesian information criterion (BIC) over the space of \mathcal{I} -Markov equivalence classes (see Definition 3 in Appendix A.1). CAM [2] is also a score-based method using greedy search, but it is nonlinear: it assumes an additive noise model where the nonlinear functions are additive. In the original paper, CAM only addresses the observational case where additive noise models are identifiable, however code is available to support perfect interventions.

Hybrid methods combine constraint and score-based approaches. Among these, IGSP [39, 40] is a method that optimizes a score based on conditional independence tests. Contrary to GIES, this method has been shown to be consistent under the faithfulness assumption. Furthermore, this method has recently been extended to support interventions with unknown targets (UT-IGSP) [34], which are also supported by our method.

¹This turns into the BIC score when the expectation is estimated with n samples, the model has one parameter per edge (like in linear models) and $\lambda = \frac{\log n}{2n}$ [28, Section 7.2.2].

2.3 Continuous constrained optimization for structure learning

A new line of research initiated by Zheng et al. [44], which serves as basis for our work, reformulates the combinatorial problem of finding the optimal DAG as a continuous constrained-optimization problem, effectively avoiding the combinatorial search. Analogous to standard score-based approaches, these methods rely on a model f_θ parametrized by θ , though θ also encodes the graph \mathcal{G} . Central to this class of methods are both the use a *weighted adjacency matrix* $A_\theta \in \mathbb{R}_{\geq 0}^{d \times d}$ (which depends on the parameters of the model) and the acyclicity constraint introduced by Zheng et al. [44] in the context of linear models:

$$\text{Tr } e^{A_\theta} - d = 0. \quad (5)$$

The weighted adjacency matrix encodes the DAG estimator $\hat{\mathcal{G}}$ as $(A_\theta)_{ij} > 0 \iff i \rightarrow j \in \hat{\mathcal{G}}$. Zheng et al. [44] showed, in the context of linear models, that $\hat{\mathcal{G}}$ is acyclic if and only if the constraint $\text{Tr } e^{A_\theta} - d = 0$ is satisfied. The general optimization problem is then

$$\max_{\theta} \mathbb{E}_{X \sim P_X} \log f_\theta(X) - \lambda \Omega(\theta) \text{ s.t. } \text{Tr } e^{A_\theta} - d = 0, \quad (6)$$

where $\Omega(\theta)$ is a regularizing term penalizing the number of edges in $\hat{\mathcal{G}}$. This problem is then approximately solved using an augmented Lagrangian procedure, as proposed by Zheng et al. [44]. Note that the problem in Equation (6) is very similar to the one resulting from Equations (3) and (4).

Continuous-constrained methods differ in their choice of model, weighted adjacency matrix, and the specifics of their optimization procedures. For instance, NOTEARS [44] assumes a Gaussian linear model with equal variances where $\theta := W \in \mathbb{R}^{d \times d}$ is the matrix of regression coefficients, $\Omega(\theta) := \|W\|_1$ and $A_\theta := W \odot W$ is the weighted adjacency matrix. Several other methods use neural networks to model nonlinear relations via f_θ and have been shown to be competitive with classical methods [21, 45]. Some define the adjacency matrix A as a function of the weights θ of the neural networks [21, 45], while others decouple θ and A by using a Gumbel-Softmax approach to model the presence/absence of edges [18, 24]. In terms of scoring, most methods rely on maximum likelihood or variants like implicit maximum likelihood [18] and evidence lower bound [41]. Zhu and Chen [46] also rely on the acyclicity constraint, but use reinforcement learning as a search strategy to estimate the DAG. Ke et al. [19] learn a DAG from data with unknown interventions using a meta-learning approach with a similar form of acyclicity constraint. However, their work covers only discrete distribution and single node interventions. To the best of our knowledge, no work has investigated, in a general manner, the use of continuous-constrained approaches in the context of interventions as we present in the next section.

3 DCDI: Differentiable causal discovery from interventional data

In this section, we present a score for imperfect interventions, provide a theorem showing its validity, and show how it can be maximized using the continuous-constrained approach to structure learning. We also provide an extension to unknown interventions without theoretical justification.

3.1 A score for imperfect interventions

The model we consider uses neural networks to model conditional densities. Moreover, we encode the DAG \mathcal{G} with a binary adjacency matrix $M^\mathcal{G} \in \{0, 1\}^{d \times d}$ which acts as a mask on the neural networks inputs. In line with the definition of interventions in Equation (2), we model the joint density of the k th intervention by

$$f^{(k)}(x; M^\mathcal{G}, \phi) := \prod_{j \notin I_k} \tilde{f}(x_j; \text{NN}(M_j^\mathcal{G} \odot x; \phi_j^{(1)})) \prod_{j \in I_k} \tilde{f}(x_j; \text{NN}(M_j^\mathcal{G} \odot x; \phi_j^{(k)})), \quad (7)$$

where $\phi := \{\phi^{(1)}, \dots, \phi^{(K)}\}$, the NN's are neural networks parameterized by $\phi_j^{(1)}$ or $\phi_j^{(k)}$ (depending on whether j is in the interventional target I_k or not), the operator \odot denotes the Hadamard product (element-wise) and $M_j^\mathcal{G}$ denotes the j th column of $M^\mathcal{G}$, which enables selecting the parents of node j in the graph \mathcal{G} . The neural networks output the parameters of a density function \tilde{f} , which in principle, could be any density. We experiment with Gaussian distributions and more expressive normalizing flows (see Section 3.4).

We propose maximizing the following regularized maximum log-likelihood score

$$\mathcal{S}_{\text{int}}(\mathcal{G}) := \max_{\phi} \sum_{k=1}^K \mathbb{E}_{X \sim p^{(k)}} \log f^{(k)}(X; M^{\mathcal{G}}, \phi) - \lambda |\mathcal{G}|, \quad (8)$$

where $p^{(k)}$ stands for the k th ground truth interventional distribution from which the data is sampled. Intuitively, this score favors graphs in which a conditional $p(x_j | x_{\pi_j^{\mathcal{G}}})$ is invariant across all interventional distributions in which x_j is not a target, i.e., $j \notin I_k$.

We now present our theoretical result (see Appendix A.2 for the proof). This theorem states that, under appropriate assumptions, maximizing $\mathcal{S}_{\text{int}}(\mathcal{G})$ yields an estimated DAG $\hat{\mathcal{G}}$ that is \mathcal{I} -Markov equivalent to the true DAG \mathcal{G}^* (see Definition 3 in Appendix A.1).

Theorem 1 *Let \mathcal{G}^* be the ground truth DAG and $\hat{\mathcal{G}} \in \arg \max_{\mathcal{G} \in \text{DAG}} \mathcal{S}_{\text{int}}(\mathcal{G})$. Under Assumptions 1 & 2 (Appendix A.2) and for $\lambda > 0$ small enough, $\hat{\mathcal{G}}$ is \mathcal{I} -Markov equivalent to \mathcal{G}^* .*

Assumption 1 requires that the model is expressive enough while Assumption 2 requires that the ground truth distributions are \mathcal{I} -faithful to the ground truth graph (generalization of the standard faithfulness assumption to interventions).

To interpret this result, note that the \mathcal{I} -Markov equivalence class of \mathcal{G}^* tends to get smaller as we add interventional targets to the interventional family \mathcal{I} . As an example, when $\mathcal{I} = (\emptyset, \{1\}, \dots, \{d\})$, i.e., when each node is individually targeted by an intervention, \mathcal{G}^* is alone in its class and, consequently, $\hat{\mathcal{G}} = \mathcal{G}^*$. See Corollary 1 in Appendix A.1 for more details.

Perfect interventions. The score $\mathcal{S}_{\text{int}}(\mathcal{G})$ can be modified to work with perfect interventions, i.e., where the targeted nodes are completely disconnected from their parents. The idea is simple and relies on the fact that the conditionals targeted by the intervention in Equation (7) do not depend on the graph \mathcal{G} anymore. This means that these terms can be removed without affecting the maximization w.r.t. \mathcal{G} . We use this version of the score when experimenting with perfect interventions.

3.2 A continuous-constrained formulation

To allow for gradient-based stochastic optimization, we follow [18, 24] and treat the adjacency matrix $M^{\mathcal{G}}$ as *random*, where the entries $M_{ij}^{\mathcal{G}}$ are independent Bernoulli variables with success probability $\sigma(\alpha_{ij})$ (σ is the sigmoid function) and α_{ij} is a scalar parameter. We group these α_{ij} 's into a matrix $\Lambda \in \mathbb{R}^{d \times d}$. We then replace the score $\mathcal{S}_{\text{int}}(\mathcal{G})$ (8) with the following relaxation:

$$\hat{\mathcal{S}}_{\text{int}}(\Lambda) := \max_{\phi} \mathbb{E}_{M \sim \sigma(\Lambda)} \left[\sum_{k=1}^K \mathbb{E}_{X \sim p^{(k)}} \log f^{(k)}(X; M, \phi) - \lambda \|M\|_0 \right], \quad (9)$$

where we dropped the \mathcal{G} superscript in M to lighten notation. This score tends asymptotically to $\mathcal{S}_{\text{int}}(\mathcal{G})$ as $\sigma(\Lambda)$ concentrates more and more its mass on \mathcal{G} .² While the expectation of the log-likelihood term is intractable, the expectation of the regularizing term simply evaluates to $\lambda \|\sigma(\Lambda)\|_1$. This score can then be maximized under the acyclicity constraint presented in Section 2.3:

$$\max_{\Lambda} \hat{\mathcal{S}}_{\text{int}}(\Lambda) \quad \text{s.t.} \quad \text{Tr } e^{\sigma(\Lambda)} - d = 0. \quad (10)$$

This problem presents two main challenges: it is a constrained problem and it contains intractable expectations. As proposed by [44], we rely on the *augmented Lagrangian* procedure to optimize ϕ and Λ jointly under the acyclicity constraint. This procedure transforms the constrained problem into a sequence of unconstrained subproblems which can themselves be optimized via a standard stochastic gradient descent algorithm for neural networks such as RMSprop. The procedure should converge to a stationary point of the original constrained problem (which is not necessarily the global optimum due to the non-convexity of the problem). In Appendix B.3, we give details on the augmented Lagrangian procedure and show the learning process in details with a concrete example.

The gradient of the likelihood part of $\hat{\mathcal{S}}_{\text{int}}(\Lambda)$ w.r.t. Λ is estimated using the Straight-Through Gumbel estimator which amounts to using Bernoulli samples in the forward pass and Gumbel-Softmax samples

²In practice, we observe that $\sigma(\Lambda)$ tends to become deterministic as we optimize.

in the backward pass which can be differentiated w.r.t. Λ via the reparametrization trick [17, 22]. This approach was already shown to give good results in the context of continuous optimization for causal discovery in the purely observational case [24, 18]. We emphasize that our approach belongs to the general framework presented in Section 2.3 where the global parameter θ is $\{\phi, \Lambda\}$, the weighted adjacency matrix A_θ is $\sigma(\Lambda)$ and the regularizing term $\Omega(\theta)$ is $\|\sigma(\Lambda)\|_1$.

3.3 Unknown interventions

Until now we have assumed that the interventional targets I_k are known. For the case where they are unknown, we propose a simple modification to our score by adding a random binary matrix $R \in \{0, 1\}^{K \times d}$, where $R_{kj} = 1$ means that X_j is a target in I_k . Similarly to the matrix M , each entry R_{kj} follows independent Bernoulli distribution with probability $\sigma(\beta_{kj})$ where β_{kj} are parameters that are learned. The likelihood is then:

$$f^{(k)}(x; M, R, \phi) := \prod_{j=1}^d \tilde{f}(x_j; \text{NN}(M_j \odot x; \phi_j^{(1)}))^{1-R_{kj}} \tilde{f}(x_j; \text{NN}(M_j \odot x; \phi_j^{(k)}))^{R_{kj}}. \quad (11)$$

The resulting score is close to (9), but the expectation is taken w.r.t. to M and R . Also, a regularization term $-\lambda_R \|R\|_0$ is added to encourage the sparsity of the learned interventional targets. Similarly to Λ , the Straight-Through Gumbel estimator is used to estimate the gradient of the score w.r.t. the parameters β_{kj} . For perfect interventions, we adapt this score by completely masking the input of the neural networks under interventions. In related work, Ke et al. [19] also use neural networks, but they support only *single* unknown target interventions and they estimate the gradient w.r.t. Λ using the log-trick which is known to have high variance [31] compared to reparameterized gradient [22].

3.4 DCDI with normalizing flows

In this section, we describe how the scores presented in Sections 3.2 & 3.3 can accommodate powerful density approximators. In the purely observational setting, very expressive models usually hinder identifiability, but given enough interventions, this is not a problem anymore. There are many possibilities when it comes to the choice of the density function \tilde{f} . In this paper, we experimented with simple Gaussian distributions as well as *normalizing flows* [30] which can represent complex causal relationships, e.g., multi-modal distributions that can occur in the presence of latent variables that are parent of only one variable.

A normalizing flow $\tau(\cdot; \omega)$ is an invertible function (e.g., a neural network) parameterized by ω with a tractable Jacobian, which can be used to model complex densities by transforming a simple random variable via the change of variable formula:

$$\tilde{f}(z; \omega) := \left| \det \left(\frac{\partial \tau(z; \omega)}{\partial z} \right) \right| p(\tau(z; \omega)), \quad (12)$$

where $\frac{\partial \tau(z; \omega)}{\partial z}$ is the Jacobian matrix of $\tau(\cdot; \omega)$ and $p(\cdot)$ is a simple density function, e.g., a Gaussian. The function $\tilde{f}(\cdot; \omega)$ can be plugged directly into the scores presented earlier by letting the neural networks $\text{NN}(\cdot; \phi_j^{(k)})$ output the parameter ω_j of the normalizing flow τ_j for each variable x_j . In our implementation, we use *deep sigmoidal flows* (DSF), a specific instantiation of normalizing flows which is a universal density approximator [15]. Details about DSF are relayed to Appendix B.2.

4 Experiments

We tested DCDI with Gaussian densities (DCDI-G) and with normalizing flows (DCDI-DSF) on a real-world data set and several synthetic data sets. The real-world task is a flow cytometry data set from Sachs et al. [32]. Our results, reported in Appendix C.1, show that our approach performs comparably to state-of-the-art methods. In this section, we focus on synthetic data sets, since these allow for a more systematic comparison of methods against various factors of variation (type of interventions, graph size, density, type of mechanisms).

We consider synthetic data sets with three interventional settings: perfect/known, imperfect/known, and perfect/unknown. Each data set has one of the three different types of causal mechanisms: i)

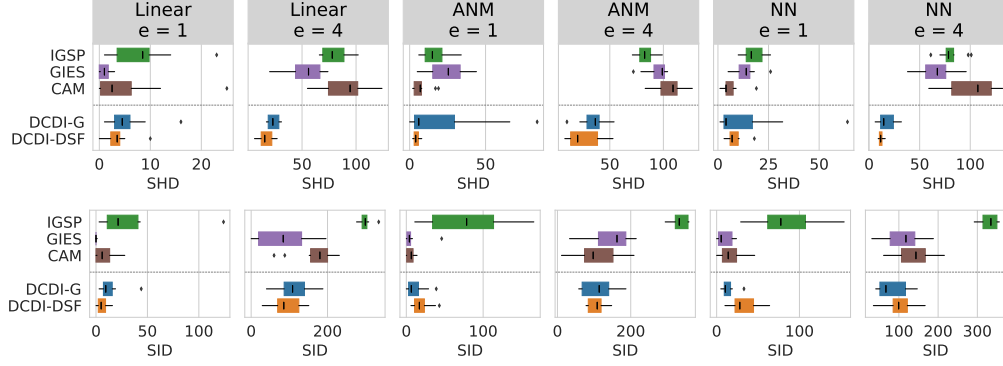


Figure 2: **Perfect interventions.** SHD and SID (lower is better) for 20-node graphs

linear [34], ii) nonlinear additive noise model (ANM) [2], and iii) nonlinear with non-additive noise using neural networks (NN) [18]. For each data set type, graphs vary in size ($d = 10$ or 20) and density ($e = 1$ or 4 where $e \cdot d$ is the average number of edges). For conciseness, we present results for 20-node graphs in the main text and report results on 10-node graphs in Appendix C.6; conclusions are similar for all sizes. For each condition, ten graphs are sampled with their causal mechanisms and then observational and interventional data are generated. Each data set has 10000 samples uniformly distributed in the different interventional settings. A total of d interventions were performed, each by sampling up to $0.1d$ target nodes. For more details on the generation process, see Appendix B.1.

Most methods have an hyperparameter controlling DAG sparsity. Although performance is sensible to this hyperparameter, many papers do not specify how it was selected. For score-based methods (GIES, CAM and DCDI), we select it by maximizing the held-out likelihood as explained in Appendix B.5 (without using the ground truth DAG). In contrast, for constraint-based methods (IGSP and UT-IGSP), we use a fixed cutoff parameter ($\alpha = 1e^{-3}$) that yielded overall good results since they do not have a likelihood model to evaluate on held-out data. We report additional results with different cutoff values in Appendix C.6. For these methods, we always pick the most advantageous independence test: partial correlation test for Gaussian linear data and KCI-test [42] for nonlinear data.

The performance of each method is assessed by two metrics on the estimated graph compared to the ground truth graph: i) the *structural Hamming distance* (SHD) which is simply the number of edges that differ between two DAGs (either reversed, missing or superfluous) and ii) the *structural interventional distance* (SID) which assesses how two DAGs differ with respect to their causal inference statements [26]. To further demonstrate the benefits of using interventional data and the usefulness of our new objective, we report an ablation study in C.4. Our implementation is available [here](#) and additional information about the baseline methods is provided in Appendix B.4.

4.1 Results for different intervention types

Perfect interventions. We compare our methods to GIES [12], a modified version of CAM [2] that support interventions and IGSP [39]. The conditionals of targeted nodes were replaced by the marginal $\mathcal{N}(2, 1)$ similarly to [12, 34]. Boxplots for SHD and SID over 10 graphs are shown in Figure 2. For all conditions, DCDI-G and DCDI-DSF shows competitive results in term of SHD and SID. For graphs with a higher number of average edges, DCDI-G and DCDI-DSF outperform all methods. GIES often shows the best performance for the linear data set, which is not surprising given that it makes the right assumptions, i.e., linear functions with Gaussian noise.

Imperfect interventions. Our conclusions are similar to the perfect intervention setting. As shown in Figure 3, DCDI-G and DCDI-DSF show competitive results and outperform other methods for graphs with a higher connectivity. The nature of the imperfect interventions are explained in Appendix B.1.

Perfect unknown interventions. We compare to UT-IGSP [34], an extension of IGSP that deal with unknown interventions. The data used are the same as in the perfect intervention setting, but the intervention targets are hidden. Results are shown in Figure 4. Except for linear data sets with sparse graphs, DCDI-G and DCDI-DSF show an overall better performance than UT-IGSP.

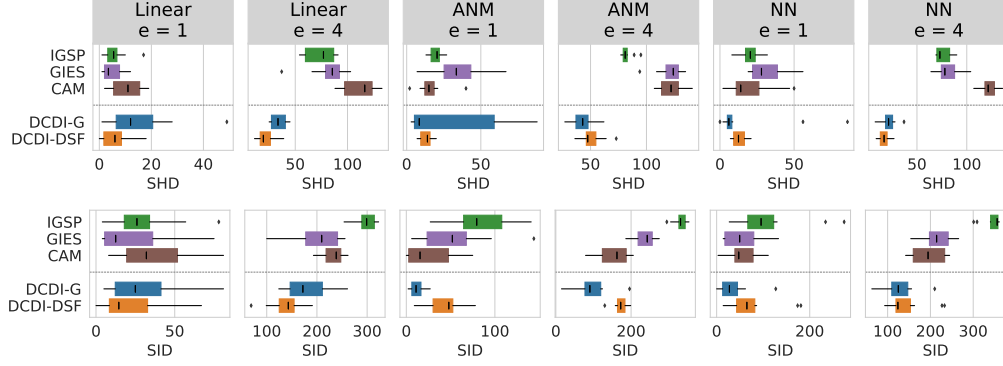


Figure 3: **Imperfect interventions.** SHD and SID for 20-node graphs

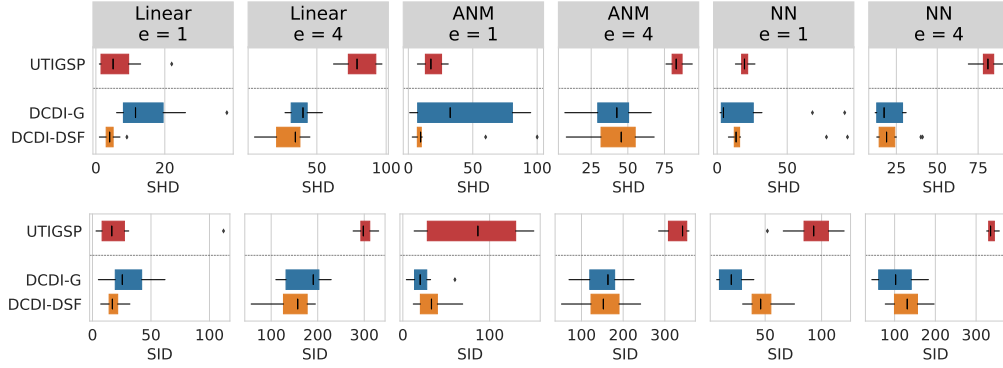


Figure 4: **Unknown interventions.** SHD and SID for 20-node graphs

Summary. For all intervention settings, DCDI has overall the best performance. In Appendix C.5, we show similar results for different types of perfect/imperfect interventions. While the advantage of DCDI-DSF over DCDI-G is marginal, it might be explained by the fact that the densities can be sufficiently well modeled by DCDI-G. In Appendix C.2, we illustrate the benefits of using high capacity estimators in this context. We show cases where methods without sufficient capacity, such as DCDI-G, fail to detect the right causal direction, whereas DCDI-DSF systematically succeeds.

4.2 Scalability experiments

So far the experiments focused on moderate size data sets, both in terms of number of variables (10 or 20) and number of examples ($\approx 10^4$). In Appendix C.3, we compare the running times of DCDI to those of other methods on graphs of up to 100 nodes and on data sets of up to 1 million examples.

The augmented Lagrangian procedure on which DCDI relies requires the computation of the matrix exponential at each gradient step, which costs $O(d^3)$. We found this does not prevent DCDI from being applied to 100 nodes graphs. Several constraint-based methods use kernel-based conditional independence tests [42, 10], which scale poorly with the number of examples. For example, KCI-test scales in $O(n^3)$ [35] and HSIC in $O(n^2)$ [43]. On the other hand, DCDI is not greatly affected by the sample size since it relies on stochastic gradient descent which is known to scale well with the data set size [1]. Our comparison shows that, among all considered methods, DCDI is the only one supporting nonlinear relationships that can scale to as much as one million examples. We believe that this can open the way to new applications of causal discovery where data is abundant.

5 Conclusion

We proposed a general continuous-constrained method for causal discovery which can leverage various types of interventional data as well as expressive neural architectures, such as normalizing flows. This approach is rooted in a sound theoretical framework and is competitive with other state-

of-the-art algorithms on real and simulated data sets, both in terms of graph recovery and scalability. This work opens interesting opportunities for future research. One direction is to extend DCDI to time-series data, where non-stationarities can be modeled as unknown interventions [29]. Another exciting direction is to learn representations of variables across multiple systems that could serve as prior knowledge for causal discovery in low data settings.

Acknowledgments

This research was partially supported by the Canada CIFAR AI Chair Program, by an IVADO excellence PhD scholarship and by a Google Focused Research award. The experiments were in part enabled by computational resources provided by Element AI, Calcul Quebec, Compute Canada. The authors would like to thank Nicolas Chapados, Rémi Lepriol, Damien Scieur and Assya Trofimov for their useful comments on the writing, Jose Gallego and Brady Neal for reviewing the proof of Theorem 1, and Grace Abuhamad for useful comments on the statement of broader impact. Simon Lacoste-Julien is a CIFAR Associate Fellow in the Learning in Machines & Brains program.

Broader impact

Causal structure learning algorithms are general tools that address two high-level tasks: *understanding* and *acting*. That is, they can help a user understand a complex system and, once such an understanding is achieved, they can help in recommending actions. We envision positive impacts of our work in fields such as scientific investigation (e.g., interpreting and anticipating the outcome of experiments), policy making for decision-makers (e.g., identifying actions that could stimulate economic growth), and improving policies in autonomous agents (e.g., learning causal relationships in the world via interaction). As a concrete example, consider the case of gene knockouts/knockdowns experiments in the field of genomics, which aim to understand how specific genes and diseases interact [47]. Learning causal models using interventions performed in this setting could help gain precious insight into gene pathways, which may catalyze the development of better pharmaceutical targets and broaden our understanding of complex diseases such as cancer. Of course, applications are likely to extend beyond these examples which seem natural from our current position.

Like any methodological contribution, our work is not immune to undesirable applications that could have negative impacts. For instance, it would be possible, yet unethical for a policy-maker to use our algorithm to understand how specific human-rights violations can reduce crime and recommend their enforcement. The burden of using our work within ethical and benevolent boundaries would rely on the user. Furthermore, even when used in a positive application, our method could have unintended consequences if used without understanding its assumptions.

In order to use our method correctly, it is crucial to understand the assumptions that it makes about the data. When such assumptions are not met, the results may still be valid, but should be used as a support to decision rather than be considered as the absolute truth. These assumptions are:

- Causal sufficiency: there are no hidden confounding variables
- The samples for a given interventional distribution are independent and identically distributed
- The causal relationships form an acyclic graph (no feedback loops)
- Our theoretical results are valid in the infinite-data regime

We encourage users to be mindful of this and to carefully analyze their results before making decisions that could have a significant downstream impact.

References

- [1] L. Bottou. Large-scale machine learning with stochastic gradient descent. In *Proceedings of COMPSTAT'2010*. 2010.
- [2] P. Bühlmann, J. Peters, and J. Ernest. Cam: Causal additive models, high-dimensional order search and penalized regression. *The Annals of Statistics*, 2014.

- [3] D. M. Chickering. Optimal structure identification with greedy search. In *Journal of Machine Learning Research*, 2003.
- [4] A. Dixit, O. Parnas, B. Li, J. Chen, C. P. Fulco, L. Jerby-Arnon, N. D. Marjanovic, D. Dionne, T. Burks, R. Raychndhury, T. M. Adamson, B. Norman, E. S. Lander, J. S. Weissman, N. Friedman, and A. Regev. Perturb-seq: dissecting molecular circuits with scalable single-cell rna profiling of pooled genetic screens. *Cell*, 2016.
- [5] D. Eaton and K. Murphy. Exact bayesian structure learning from uncertain interventions. In *Artificial intelligence and statistics*, 2007.
- [6] F. Eberhardt. Causation and intervention. *Unpublished doctoral dissertation, Carnegie Mellon University*, 2007.
- [7] F. Eberhardt. Almost Optimal Intervention Sets for Causal Discovery. In *Proceedings of the 24th Conference on Uncertainty in Artificial Intelligence*, 2008.
- [8] F. Eberhardt and R. Scheines. Interventions and causal inference. *Philosophy of Science*, 2007.
- [9] F. Eberhardt, C. Glymour, and R. Scheines. On the Number of Experiments Sufficient and in the Worst Case Necessary to Identify all Causal Relations among N Variables. In *Proceedings of the 21st Conference on Uncertainty in Artificial Intelligence*, 2005.
- [10] K. Fukumizu, A. Gretton, X. Sun, and B. Schölkopf. Kernel measures of conditional dependence. In *Advances in neural information processing systems*, 2008.
- [11] X. Glorot and Y. Bengio. Understanding the difficulty of training deep feedforward neural networks. In *Proceedings of the thirteenth international conference on artificial intelligence and statistics*, 2010.
- [12] A. Hauser and P. Bühlmann. Characterization and greedy learning of interventional markov equivalence classes of directed acyclic graphs. *Journal of Machine Learning Research*, 2012.
- [13] C. Heinze-Deml, M. H. Maathuis, and N. Meinshausen. Causal structure learning. *Annual Review of Statistics and Its Application*, 2018.
- [14] C. Heinze-Deml, J. Peters, and N. Meinshausen. Invariant causal prediction for nonlinear models. *Journal of Causal Inference*, 2018.
- [15] C.-W. Huang, D. Krueger, A. Lacoste, and A. Courville. Neural autoregressive flows. In *Proceedings of the 35th International Conference on Machine Learning*, 2018.
- [16] A. Hyttinen, F. Eberhardt, and M. Järvisalo. Constraint-based causal discovery: Conflict resolution with answer set programming. In *Proceedings of the Thirtieth Conference on Uncertainty in Artificial Intelligence*, 2014.
- [17] E. Jang, S. Gu, and B. Poole. Categorical reparameterization with gumbel-softmax. *Proceedings of the 34th International Conference on Machine Learning*, 2017.
- [18] D. Kalainathan, O. Goudet, I. Guyon, D. Lopez-Paz, and M. Sebag. Sam: Structural agnostic model, causal discovery and penalized adversarial learning. *arXiv preprint arXiv:1803.04929*, 2018.
- [19] N. R. Ke, O. Bilaniuk, A. Goyal, S. Bauer, H. Larochelle, C. Pal, and Y. Bengio. Learning neural causal models from unknown interventions. *arXiv preprint arXiv:1910.01075*, 2019.
- [20] K. B. Korb, L. R. Hope, A. E. Nicholson, and K. Axnick. Varieties of causal intervention. In *Pacific Rim International Conference on Artificial Intelligence*, 2004.
- [21] S. Lachapelle, P. Brouillard, T. Deleu, and S. Lacoste-Julien. Gradient-based neural DAG learning. In *Proceedings of the 8th International Conference on Learning Representations*, 2020.

- [22] C. J. Maddison, A. Mnih, and Y. W. Teh. The concrete distribution: A continuous relaxation of discrete random variables. *Proceedings of the 34th International Conference on Machine Learning*, 2017.
- [23] J. M. Mooij, S. Magliacane, and T. Claassen. Joint causal inference from multiple contexts. *arXiv preprint arXiv:1611.10351*, 2016.
- [24] I. Ng, Z. Fang, S. Zhu, Z. Chen, and J. Wang. Masked gradient-based causal structure learning. *arXiv preprint arXiv:1910.08527*, 2019.
- [25] J. Pearl. *Causality*. Cambridge university press, 2009.
- [26] J. Peters and P. Bühlmann. Structural intervention distance (SID) for evaluating causal graphs. *Neural Computation*, 2015.
- [27] J. Peters, P. Bühlmann, and N. Meinshausen. Causal inference by using invariant prediction: identification and confidence intervals. *Journal of the Royal Statistical Society: Series B (Statistical Methodology)*, 2016.
- [28] J. Peters, D. Janzing, and B. Schölkopf. *Elements of Causal Inference - Foundations and Learning Algorithms*. MIT Press, 2017.
- [29] N. Pfister, P. Bühlmann, and J. Peters. Invariant causal prediction for sequential data. *Journal of the American Statistical Association*, 2019.
- [30] D. J. Rezende and S. Mohamed. Variational inference with normalizing flows. *Proceedings of the 32nd International Conference on Machine Learning*, 2015.
- [31] D. J. Rezende, S. Mohamed, and D. Wierstra. Stochastic backpropagation and approximate inference in deep generative models. In *Proceedings of the 31st International Conference on Machine Learning*, 2014.
- [32] K. Sachs, O. Perez, D. Pe’er, D. A. Lauffenburger, and G. P. Nolan. Causal protein-signaling networks derived from multiparameter single-cell data. *Science*, 2005.
- [33] P. Spirtes, C. N. Glymour, R. Scheines, and D. Heckerman. *Causation, prediction, and search*. 2000.
- [34] C. Squires, Y. Wang, and C. Uhler. Permutation-based causal structure learning with unknown intervention targets. *Proceedings of the 36th Conference on Uncertainty in Artificial Intelligence*, 2020.
- [35] E. V. Strobl, K. Zhang, and S. Visweswaran. Approximate kernel-based conditional independence tests for fast non-parametric causal discovery. *Journal of Causal Inference*, 2019.
- [36] T. Tieleman and G. Hinton. Lecture 6.5-rmsprop: Divide the gradient by a running average of its recent magnitude. *COURSERA: Neural networks for machine learning*, 2012.
- [37] S. Triantafillou and I. Tsamardinos. Constraint-based causal discovery from multiple interventions over overlapping variable sets. *Journal of Machine Learning Research*, 2015.
- [38] T. Verma and J. Pearl. Equivalence and synthesis of causal models. In *Proceedings of the Sixth Annual Conference on Uncertainty in Artificial Intelligence*, 1990.
- [39] Y. Wang, L. Solus, K. Yang, and C. Uhler. Permutation-based causal inference algorithms with interventions. In *Advances in Neural Information Processing Systems*, 2017.
- [40] K. D. Yang, A. Katcoff, and C. Uhler. Characterizing and learning equivalence classes of causal DAGs under interventions. *Proceedings of the 35th International Conference on Machine Learning*, 2018.
- [41] Y. Yu, J. Chen, T. Gao, and M. Yu. DAG-GNN: DAG structure learning with graph neural networks. In *Proceedings of the 36th International Conference on Machine Learning*, 2019.

- [42] K. Zhang, J. Peters, D. Janzing, and B. Schölkopf. Kernel-based conditional independence test and application in causal discovery. *Proceedings of the Twenty-Seventh Conference on Uncertainty in Artificial Intelligence*, 2011.
- [43] Q. Zhang, S. Filippi, A. Gretton, and D. Sejdinovic. Large-scale kernel methods for independence testing. *Statistics and Computing*, 2018.
- [44] X. Zheng, B. Aragam, P.K. Ravikumar, and E.P. Xing. Dags with no tears: Continuous optimization for structure learning. In *Advances in Neural Information Processing Systems 31*, 2018.
- [45] X. Zheng, C. Dan, B. Aragam, P. Ravikumar, and E. Xing. Learning sparse nonparametric dags. In *Proceedings of the Twenty Third International Conference on Artificial Intelligence and Statistics*, 2020.
- [46] S. Zhu and Z. Chen. Causal discovery with reinforcement learning. *Proceedings of the 8th International Conference on Learning Representations*, 2020.
- [47] A. M. Zimmer, Y. K. Pan, T. Chandrapalan, R. WM Kwong, and S. F. Perry. Loss-of-function approaches in comparative physiology: is there a future for knockdown experiments in the era of genome editing? *Journal of Experimental Biology*, 2019.

Appendix

Table of Contents

A Theory	13
A.1 Theoretical Foundations for Causal Discovery with Imperfect Interventions . . .	13
A.2 Proof of Theorem 1	15
B Additional information	18
B.1 Synthetic data sets	18
B.2 Deep Sigmoidal Flow: Architectural details	19
B.3 Optimization	19
B.4 Baseline methods	22
B.5 Default hyperparameters and hyperparameter search	23
C Additional experiments	24
C.1 Real-world data set	24
C.2 Learning causal direction from complex distributions	24
C.3 Scalability experiments	26
C.4 Ablation study	26
C.5 Different kinds of interventions	30
C.6 Comprehensive results of the main experiments	32

Contents

A Theory

A.1 Theoretical Foundations for Causal Discovery with Imperfect Interventions

Before showing results about our regularized maximum likelihood score from Section 3.1, we start by briefly presenting useful definitions and results from Yang et al. [40]. We refer the reader to the original paper for a more comprehensive introduction to these notions, examples, and proofs. Throughout the appendix, we assume that the reader is comfortable with the concept of d-separation and immorality in directed graphs. Recall that we always assume $\emptyset \in \mathcal{I}$ and $I_1 := \emptyset$. We use the notation $i \rightarrow j \in \mathcal{G}$ to indicate that the edge (i, j) is in the edge set of \mathcal{G} . Given disjoint $A, B, C \subset V$, when C d-separates A from B in graph \mathcal{G} we write $A \perp\!\!\!\perp_{\mathcal{G}} B \mid C$ and when random variables X_A and X_B are independent given X_C in distribution f , we write $X_A \perp\!\!\!\perp_f X_B \mid X_C$.

Definition 2 For a DAG \mathcal{G} and an interventional family \mathcal{I} , let

$$\mathcal{M}_{\mathcal{I}}(\mathcal{G}) := \{(f^{(k)})_{k \in [K]} \mid f^{(k)}(x_1, \dots, x_d) = \prod_{j \notin I_k} f_j^{(1)}(x_j \mid x_{\pi_j^{\mathcal{G}}}) \prod_{j \in I_k} f_j^{(k)}(x_j \mid x_{\pi_j^{\mathcal{G}}}) \quad \forall k \in [K]\}$$

Definition 2 defines a set $\mathcal{M}_{\mathcal{I}}(\mathcal{G})$ which contains all the sets of distributions $(f^{(k)})_{k \in [K]}$ which are coherent with the definition of interventions provided at Equation (2).³ Note that the assumption of causal sufficiency is implicit to this definition of interventions. Analogously to the observational case, two different DAGs \mathcal{G}_1 and \mathcal{G}_2 can induce the same interventional distributions.

³Yang et al. [40] defines $\mathcal{M}_{\mathcal{I}}(\mathcal{G})$ slightly differently, but show their definition to be equivalent to the one used here. See Lemma A.1 in Yang et al. [40]

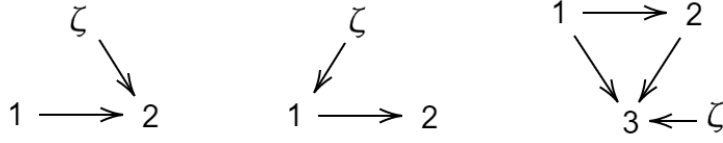


Figure 5: Different \mathcal{I} -DAGs with a single intervention. The first graph is alone in its \mathcal{I} -Markov equivalence class since reversing the $1 \rightarrow 2$ edge would break the immorality $1 \rightarrow 2 \leftarrow \zeta$. The second graph is also alone in its equivalence class since reversing $1 \rightarrow 2$ would create a new immorality $\zeta \rightarrow 1 \leftarrow 2$. The third DAG is not alone in its equivalence class since reversing $1 \rightarrow 2$ would preserve the skeleton without adding or removing an immorality. It should become apparent that adding more interventions will likely reduce the size of the \mathcal{I} -Markov equivalence class by introducing more immoralities.

Definition 3 (*\mathcal{I} -Markov Equivalence Class*) Two DAGs \mathcal{G}_1 and \mathcal{G}_2 are \mathcal{I} -Markov equivalent iff $\mathcal{M}_{\mathcal{I}}(\mathcal{G}_1) = \mathcal{M}_{\mathcal{I}}(\mathcal{G}_2)$. We denote by $\mathcal{I}\text{-MEC}(\mathcal{G}_1)$ the set of all DAGs which are \mathcal{I} -Markov equivalent to \mathcal{G}_1 , this is the \mathcal{I} -Markov equivalence class of \mathcal{G}_1 .

We now define an augmented graph containing exactly one node for each intervention k .

Definition 4 Given a DAG \mathcal{G} and an interventional family \mathcal{I} , the associated \mathcal{I} -DAG, denoted by $\mathcal{G}^{\mathcal{I}}$, is the graph \mathcal{G} augmented with nodes ζ_k and edges $\zeta_k \rightarrow i$ for all $k \in [K] \setminus \{1\}$ and all $i \in I_k$.

In the observational case, we say that a distribution f has the Markov property w.r.t. a graph \mathcal{G} if whenever some d-separation holds in the graph, the corresponding conditional independence holds in f . The next definition generalizes this idea to interventions.

Definition 5 (*\mathcal{I} -Markov property*) Let \mathcal{I} be interventional family such that $\emptyset \in \mathcal{I}$ and $(f^{(k)})_{k \in [K]}$ be a set of strictly positive densities over X . We say that $(f^{(k)})_{k \in [K]}$ satisfies the \mathcal{I} -Markov property w.r.t. the \mathcal{I} -DAG $\mathcal{G}^{\mathcal{I}}$ iff

1. For any disjoint $A, B, C \subset V$, $A \perp\!\!\!\perp_{\mathcal{G}} B | C$ implies $X_A \perp\!\!\!\perp_{f^{(k)}} X_B | X_C$ for all $k \in [K]$.
2. For any disjoint $A, C \subset V$ and $k \in [K] \setminus \{1\}$,
 $A \perp\!\!\!\perp_{\mathcal{G}^{\mathcal{I}}} \zeta_k | C \cup \zeta_{-k}$ implies $f^{(k)}(X_A | X_C) = f^{(1)}(X_A | X_C)$, where $\zeta_{-k} := \zeta_{[K] \setminus \{1, k\}}$.

The next proposition relates the definition of interventions with the \mathcal{I} -Markov property that we just defined.

Proposition 6 (Yang et al. [40]) Suppose $\emptyset \in \mathcal{I}$. Then $(f^{(k)})_{k \in [K]} \in \mathcal{M}_{\mathcal{I}}(\mathcal{G})$ iff $(f^{(k)})_{k \in [K]}$ is \mathcal{I} -Markov to $\mathcal{G}^{\mathcal{I}}$.

The next theorem gives a graphical characterization of \mathcal{I} -Markov equivalence classes.

Theorem 7 (Yang et al. [40]) Suppose $\emptyset \in \mathcal{I}$. Two DAGs \mathcal{G}_1 and \mathcal{G}_2 are \mathcal{I} -Markov equivalent iff their \mathcal{I} -DAGs $\mathcal{G}_1^{\mathcal{I}}$ and $\mathcal{G}_2^{\mathcal{I}}$ share the same skeleton and immoralities.

See Figure 5 for a simple illustration of this concept. We now present a very simple corollary which gives a situation where the \mathcal{I} -Markov equivalence class contains a unique graph.

Corollary 1 Let \mathcal{G} be a DAG and let $\mathcal{I} = (\emptyset, \{1\}, \dots, \{d\})$. Then \mathcal{G} is alone in its \mathcal{I} -Markov equivalence class.

Proof. By Theorem 7, all \mathcal{I} -Markov equivalent graphs will share its skeleton with \mathcal{G} , so we consider only graphs obtained by reversing edges in \mathcal{G} .

Consider any edge $i \rightarrow j$ in \mathcal{G} . We note that $i \rightarrow j \leftarrow \zeta_{j+1}$ forms an immorality in the \mathcal{I} -DAG $\mathcal{G}^{\mathcal{I}}$. Reversing $i \rightarrow j$ would break this immorality which would imply that the resulting DAG is not \mathcal{I} -Markov equivalent to \mathcal{G} , by Theorem 7. Hence, \mathcal{G} is alone in its equivalence class. ■

A.2 Proof of Theorem 1

We are now ready to present the main result of this section. We recall the score function introduced in Section 3.1:

$$\mathcal{S}_{\text{int}}(\mathcal{G}) := \max_{\phi} \sum_{k=1}^K \mathbb{E}_{X \sim p^{(k)}} \log f^{(k)}(X; M^{\mathcal{G}}, \phi) - \lambda |\mathcal{G}|, \quad (13)$$

$$\text{where } f^{(k)}(x; M^{\mathcal{G}}, \phi) := \prod_{j \notin I_k} \tilde{f}(x_j; \text{NN}(M_j^{\mathcal{G}} \odot x; \phi_j)) \prod_{j \in I_k} \tilde{f}(x_j; \text{NN}(M_j^{\mathcal{G}} \odot x; \phi_j^{(k)})). \quad (14)$$

Recall that $(p^{(k)})_{k \in [K]}$ are the ground truth interventional distributions with ground truth graph \mathcal{G}^* . We define $\mathcal{F}_{\mathcal{I}}(\mathcal{G})$ to be the set of all $(f^{(k)})_{k \in [K]}$ which are expressible by the model specified in Equation (14). More precisely,

$$\mathcal{F}_{\mathcal{I}}(\mathcal{G}) := \{(f^{(k)})_{k \in [K]} \mid \exists \phi \text{ s.t. } \forall k \in [K] \ f^{(k)}(x) = f^{(k)}(x; M^{\mathcal{G}}, \phi)\}. \quad (15)$$

It should be clear from the definitions that $\mathcal{F}_{\mathcal{I}}(\mathcal{G}) \subset \mathcal{M}_{\mathcal{I}}(\mathcal{G})$. Thus, from Proposition 6 we see that the \mathcal{I} -Markov property holds for all $(f^{(k)})_{k \in [K]} \in \mathcal{F}_{\mathcal{I}}(\mathcal{G})$. This fact will be useful in the proof of Theorem 1.

Theorem 1 relies on two assumptions. The first one requires that model is expressive enough to represent the ground truth distributions exactly and the second one is a faithfulness assumption similar in spirit to those encountered in standard structure learning.

Assumption 1 (*Sufficient capacity*) *The model specified in Equation (14) is expressive enough to represent the ground truth distributions, i.e. $(p^{(k)})_{k \in [K]} \in \mathcal{F}_{\mathcal{I}}(\mathcal{G}^*)$. Moreover, we assume each $p^{(k)}$ has finite entropy.*

Assumption 2 (*\mathcal{I} -Faithfulness*)

1. For any disjoint $A, B, C \subset V$,

$$A \not\perp_{\mathcal{G}^*} B | C \text{ implies } \exists k \in [K] \text{ s.t. } X_A \not\perp_{p^{(k)}} X_B | X_C.$$

2. For any disjoint $A, C \subset V$ and $k \in [K]$,

$$A \not\perp_{\mathcal{G}^*} \zeta_k | C \cup \zeta_{-k} \text{ implies } p^{(k)}(X_A | X_C) \neq p^{(1)}(X_A | X_C).$$

The first condition resembles the standard faithfulness assumption, except that we only require that the corresponding conditional independence does not hold in a given intervention distribution. The second condition is simply the converse of the second condition in the \mathcal{I} -Markov property (Definition 5).

The next lemma shows that the difference $\mathcal{S}_{\text{int}}(\mathcal{G}^*) - \mathcal{S}_{\text{int}}(\mathcal{G})$ can be rewritten as a minimization of a sum of KL divergences plus the difference in regularizing terms. We slightly compress the notation by dropping the int subscript and writing $f_{\mathcal{G}\phi}^{(k)}$ to refer the model joint $f^{(k)}(x; \mathcal{G}, \phi)$.

Lemma 8 *Under Assumption 1, we have*

$$\mathcal{S}(\mathcal{G}^*) - \mathcal{S}(\mathcal{G}) = \min_{\phi} \sum_{k \in [K]} D_{KL}(p^{(k)} || f_{\mathcal{G}\phi}^{(k)}) + \lambda(|\mathcal{G}| - |\mathcal{G}^*|). \quad (16)$$

Proof.

$$\mathcal{S}(\mathcal{G}^*) - \mathcal{S}(\mathcal{G}) = \mathcal{S}(\mathcal{G}^*) - \sum_{k \in [K]} \mathbb{E}_{p^{(k)}} \log p^{(k)}(X) - \mathcal{S}(\mathcal{G}) + \sum_{k \in [K]} \mathbb{E}_{p^{(k)}} \log p^{(k)}(X) \quad (17)$$

$$\begin{aligned} &= \max_{\phi} \sum_{k \in [K]} \mathbb{E}_{p^{(k)}} \log f_{\mathcal{G}^* \phi}^{(k)}(X) - \sum_{k \in [K]} \mathbb{E}_{p^{(k)}} \log p^{(k)}(X) \\ &\quad - \max_{\phi} \sum_{k \in [K]} \mathbb{E}_{p^{(k)}} \log f_{\mathcal{G} \phi}^{(k)}(X) + \sum_{k \in [K]} \mathbb{E}_{p^{(k)}} \log p^{(k)}(X) \\ &\quad + \lambda(|\mathcal{G}| - |\mathcal{G}^*|) \end{aligned} \quad (18)$$

$$\begin{aligned} &= \min_{\phi} - \sum_{k \in [K]} \mathbb{E}_{p^{(k)}} \log f_{\mathcal{G} \phi}^{(k)}(X) + \sum_{k \in [K]} \mathbb{E}_{p^{(k)}} \log p^{(k)}(X) \\ &\quad - \min_{\phi} - \sum_{k \in [K]} \mathbb{E}_{p^{(k)}} \log f_{\mathcal{G}^* \phi}^{(k)}(X) - \sum_{k \in [K]} \mathbb{E}_{p^{(k)}} \log p^{(k)}(X) \\ &\quad + \lambda(|\mathcal{G}| - |\mathcal{G}^*|) \end{aligned} \quad (19)$$

$$\begin{aligned} &= \min_{\phi} \sum_{k \in [K]} D_{KL}(p^{(k)} || f_{\mathcal{G} \phi}^{(k)}) - \min_{\phi} \sum_{k \in [K]} D_{KL}(p^{(k)} || f_{\mathcal{G}^* \phi}^{(k)}) \\ &\quad + \lambda(|\mathcal{G}| - |\mathcal{G}^*|) \end{aligned} \quad (20)$$

By Assumption 1 $(p^{(k)})_{k \in [K]} \in \mathcal{F}_{\mathcal{I}}(\mathcal{G}^*)$ which implies that $\min_{\phi} \sum_{k \in [K]} D_{KL}(p^{(k)} || f_{\mathcal{G}^* \phi}^{(k)}) = 0$. ■

The following definition will be useful for the next lemma.

Definition 9 Given a DAG \mathcal{G} with node set V and two nodes $i, j \in V$, we define the following sets:

$$T_{ij}^{\mathcal{G}} := \{\ell \in V \mid \text{the immorality } i \rightarrow \ell \leftarrow j \text{ is in } \mathcal{G}\} \quad (21)$$

$$L_{ij}^{\mathcal{G}} := \mathbf{DE}_{\mathcal{G}}(T_{ij}^{\mathcal{G}}) \cup \{i, j\}, \quad (22)$$

where $\mathbf{DE}_{\mathcal{G}}(S)$ is the set of descendants of S in \mathcal{G} , including S itself.

Lemma 10 Let \mathcal{G} be a DAG with node set V . When $i \rightarrow j \notin \mathcal{G}$ and $i \leftarrow j \notin \mathcal{G}$ we have

$$i \perp\!\!\!\perp_{\mathcal{G}} j \mid V \setminus L_{ij}^{\mathcal{G}}. \quad (23)$$

Proof: By contradiction. Suppose there is a path from $(i = a_0, a_1, \dots, a_p = j)$ with $p > 1$ which is not d-blocked by $V \setminus L_{ij}^{\mathcal{G}}$ in \mathcal{G} . We first consider the case where the path contains no colliders.

If the path contains no colliders, then $a_0 \leftarrow a_1$ or $a_{p-1} \rightarrow a_p$. Moreover, since the path is not d-blocked and both a_1 and a_{p-1} are not colliders, $a_1, a_{p-1} \in L_{ij}^{\mathcal{G}}$. But this implies that there is a directed path from $i = a_0$ to a_1 and a directed path from $j = a_p$ to a_{p-1} . This creates a directed cycle: either $a_0 \rightarrow \dots \rightarrow a_1 \rightarrow a_0$ or $a_p \rightarrow \dots \rightarrow a_{p-1} \rightarrow a_p$. This is a contradiction since \mathcal{G} is acyclic.

Suppose there is a collider a_k , i.e. $a_{k-1} \rightarrow a_k \leftarrow a_{k+1}$. Since the path is not d-blocked, there must exist a node $z \in \mathbf{DE}_{\mathcal{G}}(a_k) \cup \{a_k\}$ such that $z \notin L_{ij}^{\mathcal{G}}$. If $i = a_{k-1}$ and $j = a_{k+1}$, then clearly $z \in L_{ij}^{\mathcal{G}}$, which is a contradiction. Otherwise, $i \neq a_{k-1}$ or $j \neq a_{k+1}$. Without loss of generality, assume $i \neq a_{k-1}$. Clearly, a_{k-1} is not a collider and since the path is not d-blocked, $a_{k-1} \in L_{ij}^{\mathcal{G}}$. But by definition, $L_{ij}^{\mathcal{G}}$ also contains all the descendants of a_{k-1} including z . Again, this is a contradiction with $z \notin L_{ij}^{\mathcal{G}}$. ■

We recall Theorem 1 from Section 3.1 and present its proof.

Theorem 1 Let \mathcal{G}^* be the ground truth DAG and $\hat{\mathcal{G}} \in \arg \max_{\mathcal{G} \in \text{DAG}} \mathcal{S}_{\text{int}}(\mathcal{G})$. Under Assumptions 1 & 2 and for $\lambda > 0$ small enough, $\hat{\mathcal{G}}$ is \mathcal{I} -Markov equivalent to \mathcal{G}^* .

Proof. It is sufficient to prove that, for all $\mathcal{G} \notin \mathcal{I}\text{-MEC}(\mathcal{G}^*)$, $\mathcal{S}(\mathcal{G}^*) > \mathcal{S}(\mathcal{G})$. We use Theorem 7 which states that $\hat{\mathcal{G}}$ is not \mathcal{I} -Markov equivalent to \mathcal{G}^* if and only if $\hat{\mathcal{G}}^{\mathcal{I}}$ does not share its skeleton or

its immoralities with $\mathcal{G}^{*\mathcal{I}}$. The proof is organized in six cases. Cases 1-2 treat when \mathcal{G} and \mathcal{G}^* do not share the same skeleton, cases 3 & 4 when their immoralities differ and cases 5 & 6 when their immoralities implying interventional nodes ζ_k differ. In almost every cases, the idea is the same:

1. Use Lemma 10 to find a d-separation which holds in $\mathcal{G}^{\mathcal{I}}$ and show it does not hold in $\mathcal{G}^{*\mathcal{I}}$;
2. Use the fact that $\mathcal{F}_{\mathcal{I}}(\mathcal{G}) \subset \mathcal{M}_{\mathcal{I}}(\mathcal{G})$, Proposition 6 and the \mathcal{I} -faithfulness assumption to obtain an invariance which holds for all $(f^{(k)})_{k \in [K]} \in \mathcal{F}_{\mathcal{I}}(\mathcal{G})$ but not in $(p^{(k)})_{k \in [K]}$;
3. Use the fact that the invariance forces $\min_{\phi} \sum_{k \in [K]} D_{KL}(p^{(k)} || f_{\mathcal{G}\phi}^{(k)})$ to be greater than zero and;
4. Conclude that $\mathcal{S}(\mathcal{G}^*) > \mathcal{S}(\mathcal{G})$ via Lemma 8.

Case 1: We consider the graphs \mathcal{G} such that there exists $i \rightarrow j \in \mathcal{G}^*$ but $i \rightarrow j \notin \mathcal{G}$ and $i \leftarrow j \notin \mathcal{G}$. Let \mathbb{G} be the set of all such \mathcal{G} . By Lemma 10, $i \perp\!\!\!\perp_{\mathcal{G}} j \mid V \setminus L_{ij}^{\mathcal{G}}$ but clearly $i \not\perp\!\!\!\perp_{\mathcal{G}^*} j \mid V \setminus L_{ij}^{\mathcal{G}^*}$. Hence, i) by \mathcal{I} -faithfulness (Assumption 2) we have $X_i \not\perp\!\!\!\perp_{p^{(k_0)}} X_j \mid X_{V \setminus L_{ij}^{\mathcal{G}}}$ for some $k_0 \in [K]$ and ii) by the \mathcal{I} -Markov property (Proposition 6) we have $X_i \perp\!\!\!\perp_{f^{(k_0)}} X_j \mid X_{V \setminus L_{ij}^{\mathcal{G}}}$ for all $(f^{(k)})_{k \in [K]} \in \mathcal{F}_{\mathcal{I}}(\mathcal{G})$. This means that $\min_{\phi} D_{KL}(p^{(k_0)} || f_{\mathcal{G}\phi}^{(k_0)}) > 0$. For notation convenience, let us define

$$\eta(\mathcal{G}) := \min_{\phi} \sum_{k \in [K]} D_{KL}(p^{(k)} || f_{\mathcal{G}\phi}^{(k)}). \quad (24)$$

Note that

$$\eta(\mathcal{G}) \geq \min_{\phi} D_{KL}(p^{(k_0)} || f_{\mathcal{G}\phi}^{(k_0)}) > 0, \quad (25)$$

where the first inequality holds by non-negativity of the KL divergence. Using Lemma 8, we can write

$$\mathcal{S}(\mathcal{G}^*) - \mathcal{S}(\mathcal{G}) = \eta(\mathcal{G}) + \lambda(|\mathcal{G}| - |\mathcal{G}^*|). \quad (26)$$

If $|\mathcal{G}| \geq |\mathcal{G}^*|$ then clearly $\mathcal{S}(\mathcal{G}^*) - \mathcal{S}(\mathcal{G}) > 0$. Let $\mathbb{G}^+ := \{\mathcal{G} \in \mathbb{G} \mid |\mathcal{G}| < |\mathcal{G}^*|\}$. To make sure we have $\mathcal{S}(\mathcal{G}^*) - \mathcal{S}(\mathcal{G}) > 0$ for all $\mathcal{G} \in \mathbb{G}^+$, we need to pick λ sufficiently small. Choosing $0 < \lambda < \min_{\mathcal{G} \in \mathbb{G}^+} \frac{\eta(\mathcal{G})}{|\mathcal{G}^*| - |\mathcal{G}|}$ is sufficient since

$$\lambda < \min_{\mathcal{G} \in \mathbb{G}^+} \frac{\eta(\mathcal{G})}{|\mathcal{G}^*| - |\mathcal{G}|} \quad (27)$$

$$\iff \lambda < \frac{\eta(\mathcal{G})}{|\mathcal{G}^*| - |\mathcal{G}|} \quad \forall \mathcal{G} \in \mathbb{G}^+ \quad (28)$$

$$\iff \lambda(|\mathcal{G}^*| - |\mathcal{G}|) < \eta(\mathcal{G}) \quad \forall \mathcal{G} \in \mathbb{G}^+ \quad (29)$$

$$\iff 0 < \eta(\mathcal{G}) + \lambda(|\mathcal{G}| - |\mathcal{G}^*|) = \mathcal{S}(\mathcal{G}^*) - \mathcal{S}(\mathcal{G}) \quad \forall \mathcal{G} \in \mathbb{G}^+. \quad (30)$$

Case 2: We consider the graphs \mathcal{G} such that there exists $i \rightarrow j \in \mathcal{G}$ but $i \rightarrow j \notin \mathcal{G}^*$ and $i \leftarrow j \notin \mathcal{G}^*$. We can assume $i \rightarrow j \in \mathcal{G}^*$ implies $i \rightarrow j \in \mathcal{G}$ or $i \leftarrow j \in \mathcal{G}$, since otherwise we are in Case 1. Hence, it means $|\mathcal{G}| > |\mathcal{G}^*|$ which in turn implies that $\mathcal{S}(\mathcal{G}^*) > \mathcal{S}(\mathcal{G})$.

Cases 1 and 2 completely cover the situations where $\mathcal{G}^{\mathcal{I}}$ and $\mathcal{G}^{*\mathcal{I}}$ do not share the same skeleton. Next, we assume that $\mathcal{G}^{\mathcal{I}}$ and $\mathcal{G}^{*\mathcal{I}}$ do have the same skeleton (which implies that $|\mathcal{G}| = |\mathcal{G}^*|$). The remaining cases treat the differences in immoralities.

Case 3: Suppose \mathcal{G}^* contains an immorality $i \rightarrow \ell \leftarrow j$ which is not present in \mathcal{G} . We first show that $\ell \notin L_{ij}^{\mathcal{G}}$. Suppose the opposite. This means ℓ is a descendant of both i and j in \mathcal{G} . Since \mathcal{G} and \mathcal{G}^* share skeleton and because $i \rightarrow \ell \leftarrow j$ is not an immorality in \mathcal{G} , we have that $i \leftarrow \ell \in \mathcal{G}$ or $\ell \rightarrow j \in \mathcal{G}$, which in both cases creates a cycle. This is a contradiction.

The path (i, ℓ, j) is not d-blocked by $V \setminus L_{ij}^{\mathcal{G}}$ in \mathcal{G}^* since $\ell \in V \setminus L_{ij}^{\mathcal{G}}$. By \mathcal{I} -faithfulness (Assumption 2), this means that $X_i \not\perp\!\!\!\perp_{p^{(k_0)}} X_j \mid X_{V \setminus L_{ij}^{\mathcal{G}}}$ for some $k_0 \in [K]$. Since \mathcal{G}^* and \mathcal{G} share the same skeleton, we know $i \rightarrow j$ and $i \leftarrow j$ are not in \mathcal{G} . Using Lemma 10 and the \mathcal{I} -Markov property (Proposition 6),

we have that $X_i \perp\!\!\!\perp_{f^{(k_0)}} X_j \mid X_{V \setminus L_{ij}^{\mathcal{G}}}$ for all $(f^{(k)})_{k \in [K]} \in \mathcal{F}_{\mathcal{I}}(\mathcal{G})$. Similarly to Case 1, this implies that $\eta(\mathcal{G}) > 0$ which in turn implies that $\mathcal{S}(\mathcal{G}^*) - \mathcal{S}(\mathcal{G}) > 0$ (using the fact $|\mathcal{G}^*| = |\mathcal{G}|$).

Case 4: Suppose \mathcal{G} contains an immorality $i \rightarrow \ell \leftarrow j$ which is not present in \mathcal{G}^* . Since \mathcal{G} and \mathcal{G}^* share the same skeleton and $\ell \notin V \setminus L_{ij}^{\mathcal{G}}$, we know there is a (potentially undirected) path (i, ℓ, j) which is not d-blocked by $V \setminus L_{ij}^{\mathcal{G}}$ in \mathcal{G}^* . By \mathcal{I} -faithfulness (Assumption 2), we know that $X_i \not\perp\!\!\!\perp_{p^{(k_0)}} X_j \mid X_{V \setminus L_{ij}^{\mathcal{G}}}$ for some $k_0 \in [K]$. However, by Lemma 10 and the \mathcal{I} -Markov property (Proposition 6), we have that $X_i \perp\!\!\!\perp_{f^{(k_0)}} X_j \mid X_{V \setminus L_{ij}^{\mathcal{G}}}$ for all $(f^{(k)})_{k \in [K]} \in \mathcal{F}_{\mathcal{I}}(\mathcal{G})$. Thus, again, $\mathcal{S}(\mathcal{G}^*) - \mathcal{S}(\mathcal{G}) > 0$.

So far, all cases did not require interventional nodes ζ_k . Cases 5 and 6 treat the difference in immoralities implying interventional nodes ζ_k . Note that the arguments are analog to cases 5 and 6.

Case 5: Suppose that there is an immorality $i \rightarrow \ell \leftarrow \zeta_j$ in $\mathcal{G}^{*\mathcal{I}}$ which does not appear in $\mathcal{G}^{\mathcal{I}}$. The path (i, ℓ, ζ_j) is not d-blocked by $\zeta_{-j} \cup V \setminus L_{i\zeta_j}^{\mathcal{G}^{\mathcal{I}}}$ in $\mathcal{G}^{*\mathcal{I}}$ since $\ell \in \zeta_{-j} \cup V \setminus L_{i\zeta_j}^{\mathcal{G}^{\mathcal{I}}}$ (by same argument as presented in Case 3). By \mathcal{I} -faithfulness (Assumption 2), this means that

$$p^{(1)}(x_i \mid x_{V \setminus L_{i\zeta_j}^{\mathcal{G}^{\mathcal{I}}}}) \neq p^{(j)}(x_i \mid x_{V \setminus L_{i\zeta_j}^{\mathcal{G}^{\mathcal{I}}}}). \quad (31)$$

On the other hand, Lemma 10 implies that $i \perp\!\!\!\perp_{\mathcal{G}^{\mathcal{I}}} \zeta_j \mid \zeta_{-j} \cup V \setminus L_{i\zeta_j}^{\mathcal{G}^{\mathcal{I}}}$. By the \mathcal{I} -Markov property (Proposition 6), we have that

$$f^{(1)}(x_i \mid x_{V \setminus L_{i\zeta_j}^{\mathcal{G}^{\mathcal{I}}}}) = f^{(j)}(x_i \mid x_{V \setminus L_{i\zeta_j}^{\mathcal{G}^{\mathcal{I}}}}) \quad \text{for all } (f^{(k)})_{k \in [K]} \in \mathcal{F}_{\mathcal{I}}(\mathcal{G}). \quad (32)$$

This means that $\mathcal{S}(\mathcal{G}^*) > \mathcal{S}(\mathcal{G})$ since

$$\mathcal{S}(\mathcal{G}^*) - \mathcal{S}(\mathcal{G}) = \min_{\phi} \sum_{k \in [K]} D_{KL}(p^{(k)} \parallel f_{\mathcal{G}\phi}^{(k)}) \quad (33)$$

$$\geq \min_{\phi} D_{KL}(p^{(1)} \parallel f_{\mathcal{G}\phi}^{(1)}) + D_{KL}(p^{(j)} \parallel f_{\mathcal{G}\phi}^{(j)}) \quad (34)$$

$$> 0, \quad (35)$$

where the last equality holds because both divergences cannot be put to zero simultaneously.

Case 6: Suppose that there is an immorality $i \rightarrow \ell \leftarrow \zeta_j$ in $\mathcal{G}^{\mathcal{I}}$ which does not appear in $\mathcal{G}^{*\mathcal{I}}$. The path (i, ℓ, ζ_j) is not d-blocked by $\zeta_{-j} \cup V \setminus L_{i\zeta_j}^{\mathcal{G}^{\mathcal{I}}}$ in $\mathcal{G}^{*\mathcal{I}}$, since $\ell \notin \zeta_{-j} \cup V \setminus L_{i\zeta_j}^{\mathcal{G}^{\mathcal{I}}}$ and both \mathcal{I} -DAGs share the same skeleton. It follows by \mathcal{I} -faithfulness (Assumption 2) that

$$p^{(1)}(x_i \mid x_{V \setminus L_{i\zeta_j}^{\mathcal{G}^{\mathcal{I}}}}) \neq p^{(j)}(x_i \mid x_{V \setminus L_{i\zeta_j}^{\mathcal{G}^{\mathcal{I}}}}). \quad (36)$$

On the other hand, Lemma 10 implies that $i \perp\!\!\!\perp_{\mathcal{G}^{\mathcal{I}}} \zeta_j \mid \zeta_{-j} \cup V \setminus L_{i\zeta_j}^{\mathcal{G}^{\mathcal{I}}}$. Again by the \mathcal{I} -Markov property (Proposition 6), it means that

$$f^{(1)}(x_i \mid x_{V \setminus L_{i\zeta_j}^{\mathcal{G}^{\mathcal{I}}}}) = f^{(j)}(x_i \mid x_{V \setminus L_{i\zeta_j}^{\mathcal{G}^{\mathcal{I}}}}) \quad \text{for all } (f^{(k)})_{k \in [K]} \in \mathcal{F}_{\mathcal{I}}(\mathcal{G}). \quad (37)$$

By an argument identical to that of Case 5, it follows that $\mathcal{S}(\mathcal{G}^*) > \mathcal{S}(\mathcal{G})$.

The proof is complete since there is no other way in which $\mathcal{G}^{\mathcal{I}}$ and $\mathcal{G}^{*\mathcal{I}}$ can differ in terms of skeleton and immoralities. ■

B Additional information

B.1 Synthetic data sets

In this section, we describe how the different synthetic data sets were generated. For each type of data set, we first sample a DAG following the *Erdős-Rényi* scheme and then we sample the parameters of

the different causal mechanisms as stated below (in the bulleted list). For 10-node graphs, single node interventions are performed on every node. For 20-node graphs, interventions target 1 to 2 nodes chosen uniformly at random. Then, $n/(d+1)$ examples are sampled for each interventional setting (if n is not divisible by $d+1$, some intervention setting may have one extra sample in order to have a total of n samples). The data are then normalized: we subtract the mean and divide by the standard deviation. For all data sets, the source nodes are Gaussian with zero mean and variance sampled from $\mathcal{U}[1, 2]$. The noise variables N_j are mutually independent and sampled from $\mathcal{N}(0, \sigma_j^2) \forall j$, where $\sigma_j^2 \sim \mathcal{U}[1, 2]$.

For perfect intervention, the distribution of intervened nodes is replaced by a marginal $\mathcal{N}(2, 1)$. This type of intervention, that produce a mean-shift, is similar to those used in [12, 34]. For imperfect interventions, besides the initial parameters, an extra set of parameters were sampled by perturbing the initial parameters as described below. For nodes without parents, the distribution of intervened nodes is replaced by a marginal $\mathcal{N}(2, 1)$. Both for the perfect and imperfect cases, we explore other types of interventions and report the results in Appendix C.5. We now describe the causal mechanisms and the nature of the imperfect intervention for the three different types of data set:

- The *linear* data sets are generated following $X_j := w_j^T X_{\pi_j^G} + 0.4 \cdot N_j \forall j$, where w_j is a vector of $|\pi_j^G|$ coefficients each sampled uniformly from $[-1, -0.25] \cup [0.25, 1]$ (to make sure there are no w close to 0). Imperfect interventions are obtained by adding a random vector of $\mathcal{U}([-5, -2] \cup [2, 5])$ to w_j .
- The *additive noise model* (ANM) data sets are generated following $X_j := f_j(X_{\pi_j^G}) + 0.4 \cdot N_j \forall j$, where the functions f_j are fully connected neural networks with one hidden layer of 10 units and *leaky ReLU* with a negative slope of 0.25 as nonlinearities. The weights of each neural network are randomly initialized from $\mathcal{N}(0, 1)$. Imperfect interventions are obtained by adding a random vector of $\mathcal{N}(0, 1)$ to the last layer.
- The *nonlinear with non-additive noise* (NN) data sets are generated following $X_j := f_j(X_{\pi_j^G}, N_j) \forall j$, where the functions f_j are fully connected neural networks with one hidden layer of 20 units and *tanh* as nonlinearities. The weights of each neural network are randomly initialized from $\mathcal{N}(0, 1)$. Similarly to the additive noise model, imperfect intervention are obtained by adding a random vector of $\mathcal{N}(0, 1)$ to the last layer.

B.2 Deep Sigmoidal Flow: Architectural details

A layer of a Deep Sigmoidal Flow is similar to a fully-connected network with one hidden layer, a single input, and a single output, but is defined slightly differently to ensure that the mapping is invertible and that the Jacobian is tractable. Each layer l is defined as follows:

$$h^{(l)}(x) = \sigma^{-1}(w^T \sigma(a \cdot x + b)), \quad (38)$$

where $0 < w_i < 1$, $\sum_i w_i = 1$ and $a_i > 0$. In our method, the neural networks $\text{NN}(\cdot; \phi_j^{(k)})$ output the parameters (w_j, a_j, b_j) for each DSF τ_j . To ensure that the determinant of the Jacobian is calculated in a numerically-stable way, we follow the recommendations of [15]. While other flows like the Deep Dense Sigmoidal Flow have more capacity, DSF was sufficient for our use.

B.3 Optimization

In this section, we show how the augmented Lagrangian is applied, how the gradient is estimated and, finally, we illustrate the learning dynamics by analyzing an example.

Let us recall the score and the optimization problem from Section 3.2:

$$\hat{S}_{\text{int}}(\Lambda) := \max_{\phi} \mathbb{E}_{M \sim \sigma(\Lambda)} \left[\sum_{k=1}^K \mathbb{E}_{X \sim p^{(k)}} \log f^{(k)}(X; M, \phi) - \lambda \|M\|_0 \right], \quad (39)$$

$$\max_{\Lambda} \hat{S}_{\text{int}}(\Lambda) \quad \text{s.t.} \quad \text{Tr } e^{\sigma(\Lambda)} - d = 0. \quad (40)$$

We optimize for ϕ and Λ jointly, which yields the following optimization problem:

$$\max_{\phi, \Lambda} \mathbb{E}_{M \sim \sigma(\Lambda)} \left[\sum_{k=1}^K \mathbb{E}_{X \sim p^{(k)}} \log f^{(k)}(X; M, \phi) \right] - \lambda \|\sigma(\Lambda)\|_1 \quad \text{s.t.} \quad \text{Tr } e^{\sigma(\Lambda)} - d = 0, \quad (41)$$

where we used the fact that $\mathbb{E}_{M \sim \sigma(\Lambda)} \|M\|_0 = \|\sigma(\Lambda)\|_1$. Let us use the notation:

$$h(\Lambda) := \text{Tr } e^{\sigma(\Lambda)} - d. \quad (42)$$

The augmented Lagrangian transforms the constrained problem into a sequence of unconstrained problems of the form

$$\max_{\phi, \Lambda} \mathbb{E}_{M \sim \sigma(\Lambda)} \left[\sum_{k=1}^K \mathbb{E}_{X \sim p^{(k)}} \log f^{(k)}(X; M, \phi) \right] - \lambda \|\sigma(\Lambda)\|_1 - \gamma_t h(\Lambda) - \frac{\mu_t}{2} h(\Lambda)^2, \quad (43)$$

where γ_t and μ_t are the Lagrangian multiplier and the penalty coefficient of the t th unconstrained problem, respectively. In all our experiments, we initialize $\gamma_0 = 0$ and $\mu_0 = 10^{-8}$. Each such problem is approximately solved using a stochastic gradient descent algorithm (RMSprop [36] in our experiments). We consider that a subproblem has converged when (43) evaluated on a held-out data set stops increasing. Let (ϕ_t^*, Λ_t^*) be the approximate solution to subproblem t . Then, γ_t and μ_t are updated according to the following rule:

$$\begin{aligned} \gamma_{t+1} &\leftarrow \gamma_t + \mu_t \cdot h(\Lambda_t^*) \\ \mu_{t+1} &\leftarrow \begin{cases} \eta \cdot \mu_t, & \text{if } h(\Lambda_t^*) > \delta \cdot h(\Lambda_{t-1}^*) \\ \mu_t, & \text{otherwise} \end{cases} \end{aligned} \quad (44)$$

with $\eta = 2$ and $\delta = 0.9$. Each subproblem t is initialized using the previous subproblem's solution $(\phi_{t-1}^*, \Lambda_{t-1}^*)$. The augmented Lagrangian method stops when $h(\Lambda) \leq 10^{-8}$ and the graph formed by adding an edge whenever $\sigma(\Lambda) > 0.5$ is acyclic.

Gradient estimation. The gradient of (43) w.r.t. ϕ and Λ is estimated by

$$\nabla_{\phi, \Lambda} \left[\frac{1}{|B|} \sum_{i \in B} \log f^{(k_i)}(x^{(i)}; M^{(i)}, \phi) - \lambda_t h(\Lambda) - \frac{\mu_t}{2} h(\Lambda)^2 \right], \quad (45)$$

where B is an index set sampled without replacement, $x^{(i)}$ is an example from the training set and k_i is the index of its corresponding intervention. To compute the gradient of the likelihood part w.r.t. Λ , we use the Straight-Through Gumbel-Softmax estimator, adapted to sigmoids [22, 17]. This approach was already used in the context of causal discovery without interventional data [24, 18]. The matrix $M^{(i)}$ is given by

$$M^{(i)} := \mathbb{I}(\sigma(\Lambda + L^{(i)}) > 0.5) + \sigma(\Lambda + L^{(i)}) - \text{grad-block}(\sigma(\Lambda + L^{(i)})), \quad (46)$$

where $L^{(i)}$ is a $d \times d$ matrix filled with independent Logistic samples, \mathbb{I} is the indicator function applied element-wise and the function *grad-block* is such that $\text{grad-block}(z) = z$ and $\nabla_z \text{grad-block}(z) = 0$. This implies that each entry of $M^{(i)}$ evaluates to a discrete Bernoulli sample with probability given by $\sigma(\Lambda)$ while the gradient w.r.t. Λ is computed using the soft Gumbel-Softmax sample. This yields a biased estimation of the actual gradient of objective (43), but its variance is low compared to the popular unbiased REINFORCE estimator (a Monte Carlo estimator relying on the log-trick) [31, 22]. A temperature term can be added inside the sigmoid, but we found that a temperature of one gave good results.

We considered a different relaxation for the discrete variable M . We tried treating M directly as a learnable parameter constrained in $[0, 1]$ via gradient projection. But this approach yielded significantly worse results. We believe the fact M is continuous is problematic, because as an entry of M gets closer and closer to zero, the weights of the first neural network layer can compensate, without affecting the likelihood whatsoever. This cannot happen when using the Straight-Through Gumbel-Softmax estimator because the neural network weights are only exposed to discrete M .

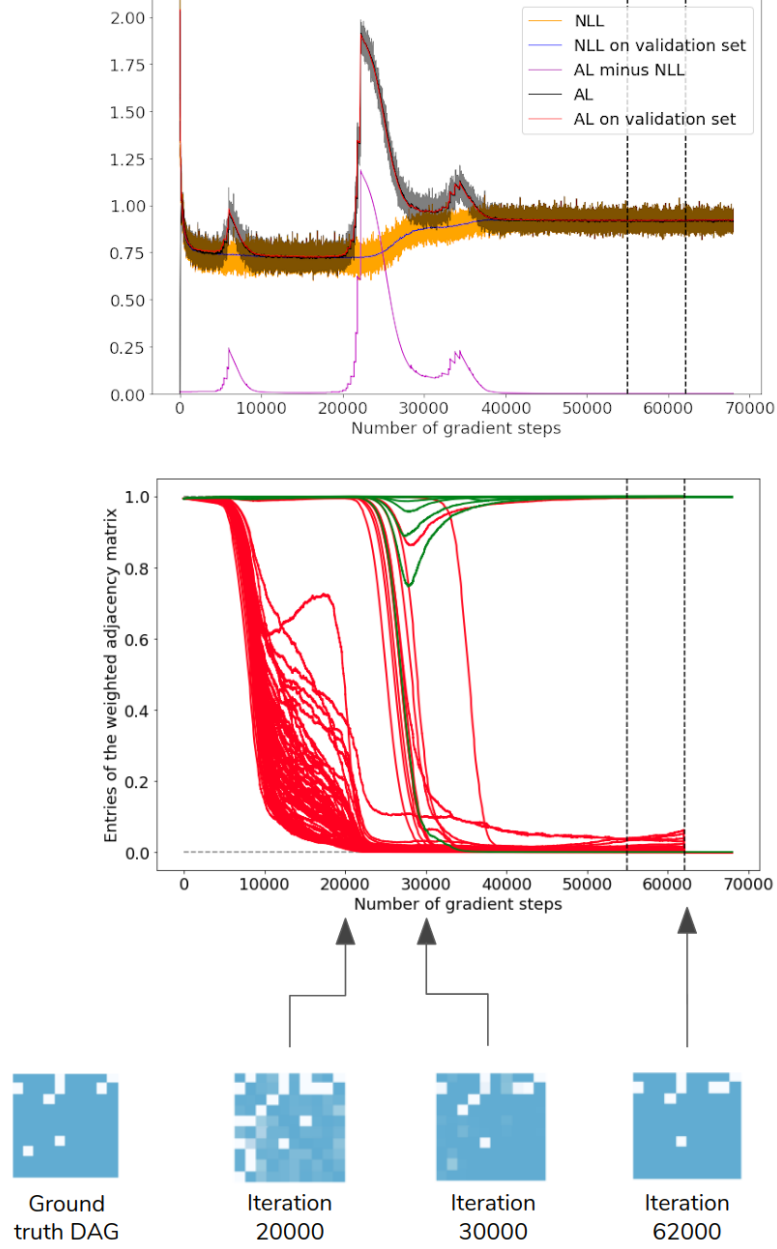


Figure 6: **Top:** Learning curves during training. *NLL* and *NLL on validation* are respectively the (pseudo) negative log-likelihood (NLL) on training and validation sets. *AL minus NLL* can be thought of as the acyclicity constraint violation plus the edge sparsity regularizer. *AL* and *AL on validation set* are the augmented Lagrangian objectives on training and validation set, respectively. **Middle and bottom:** Entries of the matrix $\sigma(\Lambda)$ w.r.t. to the number of iterations (green edges = edge present in the ground truth DAG, red edges = edge not present). The adjacency matrix to the left correspond to the ground truth DAG. The other matrices correspond to $\sigma(\Lambda)$ at 20 000, 30 000 and 62 000 iterations.

Learning dynamics. We present in Figure 6 the learning curves (top) and the matrix $\sigma(\Lambda)$ (middle and bottom) as DCDI-DSF is trained on a linear data set with perfect intervention sampled from a sparse 10-node graph (the same phenomenon was observed in a wide range of settings). In the graph at the top, we show the augmented Lagrangian and the (pseudo) negative log-likelihood (NLL) on train and validation set. To be exact, the NLL corresponds to a negative log-likelihood only once acyclicity is achieved. In the graph representing $\sigma(\Lambda)$ (middle), each curve represent a $\sigma(\alpha_{ij})$: green edges are edges present in the ground truth DAG and red edges are edges not present. The same information is presented in matrix form for a few specific iterations and can be easily compared to the adjacency matrix of the ground truth DAG (white = presence of an edge, blue = absence). Recall that when a $\sigma(\alpha_{ij})$ is equal (or close to) 0, it means that the entry ij of the mask M will also be 0. This is equivalent to say that the edge is not present in the learned DAG.

In this section we review some important steps of the learning dynamics. At first, the NLL on the training and validation sets decrease sharply as the model fits the data. Around the iteration 5000, the decrease slows down and the weights of the constraint (namely γ and μ) are increased. This puts pressure on the entries $\sigma(\alpha_{ij})$ to decrease. At iteration 20 000, many $\sigma(\alpha_{ij})$ that correspond to red edges have diminished close to 0, meaning that edges are correctly removed. It is noteworthy to mention that the matrix at this stage is close to being symmetric: the algorithm did not yet choose an orientation for the different edges. While this learned graph still has false positive edges, the skeleton is reminiscent of a Markov Equivalence Class. As the training progresses, the weights of the constraint are greatly increased passed the 20 000th iteration leading to the removal of additional edges (leading also to an NLL increase). Around iteration 62 000 (the second vertical line), the stopping criterion is met: the acyclicity constraint is below the threshold (i.e. $h(\Lambda) \leq 10^{-8}$), the learned DAG is acyclic and the augmented Lagrangian on the validation set is not improving anymore. Edges with a $\sigma(\alpha_{ij})$ higher than 0.5 are set to 1 and others set to 0. The learned DAG has a SHD of 1 since it has a reversed edge compared to the ground truth DAG.

Finally, we illustrate the learning of interventional targets in the (perfect) unknown intervention setting by comparing an example of $\sigma(\beta_{kj})$, the learned targets, with the ground truth targets in Figure 7. Results are from DCDI-G on 10-node graph with higher connectivity. Each column correspond to an interventional target I_k and each row correspond to a node. In the right matrix, a dark grey square in position ij means that the node i was intervened on in the interventional setting I_j . Each entry of the left matrix corresponds to the value of $\sigma(\beta_{kj})$. The binary matrix R (from Equation 11) is sampled following these entries.

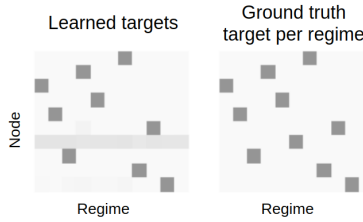


Figure 7: Learned targets $\sigma(\beta_{kj})$ compared to the ground truth targets.

B.4 Baseline methods

In this section, we provide additional details on the baseline methods and cite the implementations that were used. GIES has been designed for the perfect interventions setting. It assumes linear relations with Gaussian noise and outputs an \mathcal{I} -Markov equivalence classes. In order to obtain the SHD and SID, we compare a DAG randomly sampled from the returned \mathcal{I} -Markov equivalence classes to the ground truth DAG. CAM has been modified to support perfect interventions. In particular, we modified the loss similarly to the loss proposed for DCDI in the perfect intervention setting. Also, the preliminary neighbor search (PNS) and pruning processes were modified to not take into account data where variables are intervened on. Note that, while these two methods yield competitive results in the imperfect intervention setting, they were designed for perfect interventions: the targeted conditional are not fitted by an additional model (in contrast to our proposed score), they are simply removed from the score.

For GIES, we used the implementation from the R package `pcalg`. For CAM, we modified the implementation from the R package `pcalg`. For IGSP and UT-IGSP, we used the implementation from <https://github.com/uhlerlab/causal DAG>. The cutoff values used for α -inv was always the same as α . The normalizing flows that we used for DCDI-DSF were adapted from the DSF implementation provided by its author [15]. We also used several tools from <https://github.com/FenTechSolutions/CausalDiscoveryToolbox> to interface R with Python and to compute the SHD and SID metrics.

B.5 Default hyperparameters and hyperparameter search

For all score-based methods, we performed a hyperparameter search. The models were trained on 80% examples and evaluated on the 20% remaining examples. The hyperparameter combination chosen was the one that induced the lowest negative log-likelihood on the held-out examples. For DCDI, a grid search was performed over 10 values of the regularization coefficient (see Table 1) for known interventions (10 hyperparameter combinations in total) and, in the unknown intervention case, 3 values for the regularization coefficient of the learned targets λ_R were also explored (30 hyperparameter combinations in total). For GIES and CAM, 50 hyperparameter combinations were considered using a random search following the sampling scheme of Table 1.

For IGSP and UT-IGSP, we could not do a similar hyperparameter search since there is no score available to rank hyperparameter combinations. Thus, all examples were used to fit the model. Despite this, we explored a range of cutoff values around 10^{-5} (the value used for all the experiments in [34]): $\log_{10} \alpha = \{-2, -3, -5, -7, -9\}$. We chose 10^{-3} , which yielded low SHD and SID. Note that in a realistic setting, we do not have access to the ground truth graphs to make that decision.

Table 1: Hyperparameter search spaces for each algorithm

	Hyperparameter space
DCDI	$\log_{10}(\lambda) \sim \mathcal{U}\{-7, -6, -5, -4, -3, -2, -1, 0, 1, 2\}$
	$\log_{10}(\lambda_R) \sim \mathcal{U}\{-4, -3, -2\}$ (only for unknown interventions)
CAM	$\log_{10}(\text{pruning cutoff}) \sim \mathcal{U}[-7, 0]$
GIES	$\log_{10}(\text{regularizer coefficient}) \sim \mathcal{U}[-4, 4]$

Except for the normalizing flows of DCDI-DSF, DCDI-G and DCDI-DSF used exactly the same default hyperparameters that are summarized in Table 2. Some of these hyperparameters (μ_0, γ_0), which are related to the optimization process are presented in Appendix B.3. These hyperparameters were used for almost all experiments, except for the real-world data set and the two-node graphs with complex densities, where overfitting was observed. Smaller architectures were tested until no major overfitting was observed. The default hyperparameters were chosen using small-scale experiments on perfect-known interventions data sets in order to have a small SHD. Since we observed that DCDI is not highly sensible to changes in hyperparameter values, only the regularization factors were part of a more thorough hyperparameter search. The neural networks were initialized following the Xavier initialization [11]. The neural network activation functions were leaky-ReLU. RMSprop was used as the optimizer [36] with minibatches of size 64.

Table 2: Default Hyperparameter for DCDI-G and DCDI-DSF

DCDI hyperparameters
$\mu_0: 10^{-8}, \gamma_0: 0, \eta: 2, \delta: 0.9$
Augmented Lagrangian constraint threshold: 10^{-8}
learning rate: 10^{-3}
hidden units: 16
hidden layers: 2
flow hidden units: 16 (only for DCDI-DSF)
flow hidden layers: 2 (only for DCDI-DSF)

C Additional experiments

C.1 Real-world data set

We tested the methods that support perfect intervention on the flow cytometry data set of Sachs et al. [32]. The measurements are the level of expression of phosphoproteins and phospholipids in human cells. Interventions were performed by using reagents to activate or inhibit the measured proteins. As in Wang et al. [39], we use a subset of the data set, excluding experimental conditions where the perturbations were not directly done on a measured protein. This subset comprises 5 846 measurements: 1 755 measurements are considered observational, while the other 4 091 measurements are from five different single node interventions (with the following proteins as targets: Akt, PKC, PIP2, Mek, PIP3). The consensus graph from Sachs et al. [32] that we use as the ground truth DAG contains 11 nodes and 17 edges. While the flow cytometry data sets is standard in the causal structure learning literature, some concerns have been raised. The “consensus” network proposed by [32] has been challenged by some experts [23]. Also, several assumptions of the different models may not be respected in this real-world data set (for more details, see [23]): i) the causal sufficiency assumption may not hold, ii) the interventions may not be as specific as stated, and iii) the ground truth network is possibly not a DAG since feedback loops are common in cellular signaling networks.

Table 3: Results for the flow cytometry data sets

Method	SHD	SID	tp	fn	fp	rev	F_1 score
IGSP	18	54	4	6	5	7	0.42
GIES	38	34	10	0	41	7	0.33
CAM	35	20	12	1	30	4	0.51
DCDI-G	36	43	6	2	25	9	0.31
DCDI-DSF	33	47	6	2	22	9	0.33

In Table 3 we report SHD and SID for all methods, along with the number of true positive (tp), false negative (fn), false positive (fp), reversed (rev) edges, and the F_1 score. There are no measures of central tendencies, since there is only one graph. The modified version of CAM has overall the best performance: the highest F_1 score and a low SID. IGSP has a low SHD, but a high SID, which can be explained by the relatively high number of false negative. DCDI-G and DCDI-DSF have SHDs comparable to GIES and CAM, but higher than IGSP. In terms of SID, they outperform IGSP, but not GIES and CAM. Finally, the DCDI models have F_1 scores similar to that of GIES. Hence, we conclude that DCDI performs comparably to the state of the art on this data set, while none of the methods show great performance across the board.

Hyperparameters. We report the hyperparameters used for Table 3. IGSP used the KCI-test with a cutoff value of 10^{-3} . Hyperparameters for CAM and GIES were chosen following the hyperparameter search described in Appendix B.5. For DCDI, since overfitting was observed, we included some hyperparameters related to the architecture in the hyperparameter grid search (number of hidden units: $\{4, 8\}$, number of hidden layers: $\{1, 2\}$ and only for DSF, number of flow hidden units: $\{4, 8\}$, number of flow layers: $\{1, 2\}$), and used the scheme described in Appendix B.5 for choosing the regularization coefficient.

C.2 Learning causal direction from complex distributions

To show that insufficient capacity can hinder learning the right causal direction, we used toy data sets with simple 2-node graphs under perfect and imperfect interventions. We show, in Figure 8 and 9, the joint densities respectively learned by DCDI-DSF and DCDI-G. We tested two different data sets: X and DNA, which corresponds to the left and right column, respectively. In both data sets, we experimented with perfect and imperfect interventions, on both the cause and the effect, i.e. $\mathcal{I} = (\emptyset, \{1\}, \{2\})$. In both figures, the top row corresponds to the learned densities when no intervention are performed. The bottom row corresponds to the learned densities under an imperfect intervention on the effect variable (changing the conditional).

For the X data set, both under perfect and imperfect interventions, the incapacity of DCDI-G to model this complex distribution properly makes it conclude (falsely) that there is no dependency between the two variables (the μ outputted by DCDI-G is constant). Conversely, for the DNA data

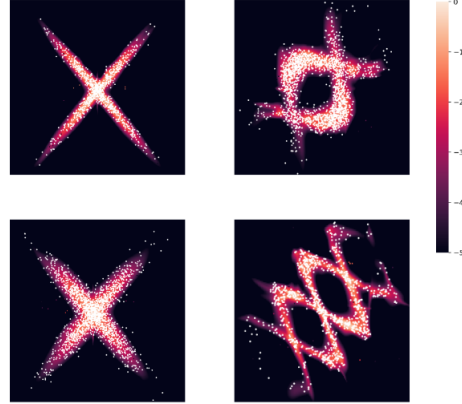


Figure 8: Joint density learned by DCDI-DSF. White dots are data points and the color represents the learned density. The x-axis is cause and the y-axis is the effect. First row is observational while second row is with an imperfect intervention on the effect.

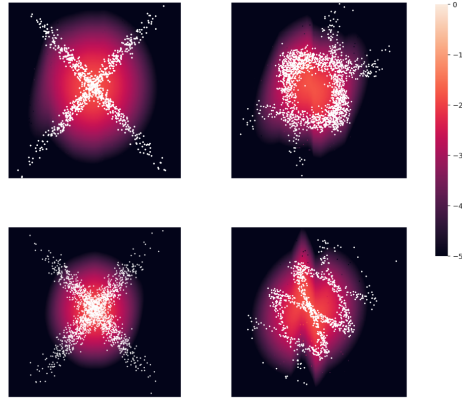


Figure 9: Joint density learned by DCDI-G. White dots are data points and the color represents the learned density. The x-axis is cause and the y-axis is the effect. First row is observational while second row is with an imperfect intervention on the effect.

set with perfect interventions, it does infer the dependencies between the two variables and learn the correct causal direction, although the distribution is modeled poorly. Notice that, for the DNA data set with imperfect interventions, the lack of capacity of DCDI-G has pushed it to learn the same density with and without interventions (compare the two densities in the second column of Figure 9; the learned density functions remain mostly unchanged from top to bottom). This prevented DCDI-G from learning the correct causal direction, while DCDI-DSF had no problem. We believe that if the imperfect interventions were more radical, DCDI-G could have recovered the correct direction even though it lacks capacity. In all cases, DCDI-DSF can easily model these functions and systematically infers the right causal direction.

While the proposed data sets are synthetic, similar multimodal distributions could be observed in real-world data sets due to latent variables that are parent of only one node (i.e., that are not confounders). A hidden variable that act as a selector between two different mechanisms could induce distributions similar to those in Figures 8 and 9. In fact, this idea was used to produce the synthetic data sets, i.e., a latent variable $z \in \{0, 1\}$ was sampled and, according to its value, example were generated following one of two mechanisms. The for the X dataset (second column in the figures) was generated by two linear mechanisms in the following way:

$$y := \begin{cases} wx + N & z = 0 \\ -wx + N & z = 1, \end{cases}$$

where N is a Gaussian noise and w was randomly sampled from $[-1, -0.25] \cup [0.25, 1]$.

C.3 Scalability experiments

Figure 10 presents two experiments which study the scalability of various methods in terms of number of examples (left) and number of variables (right). In these experiments, the runtime was restricted to 12 hours while the RAM memory was restricted to 16GB. All experiments considered perfect interventions. Experiments from Figure 10 were run with fixed hyperparameters. **DCDI**. Same as Table 2 except $\mu_0 = 10^{-2}$, # hidden units = 8 and $\lambda = 10^{-1}$. **CAM**. Pruning cutoff = 10^{-3} . Preliminary neighborhood selection was performed in the large graph experiments (otherwise CAM cannot run on 50 nodes in less than 12 hours). **GIES**. Regularizing parameter = 1. **IGSP**. The suffixes -G and -K refers to the partial correlation test and the KCI-test, respectively. The α parameter is set to 10^{-3} .

Number of examples. DCDI was the only algorithm supporting nonlinear relationships which could run on as much as 1 million examples without running out of time or memory. We believe different trade-offs between SHD and SID could be achieved with different hyperparameters, especially for GIES and CAM which achieved very good SID but poor SHD.

Number of variables. We see that using a GPU starts to pay off for graphs of 50 nodes or more. For 10-50 nodes data sets, DCDI-GPU outperforms the other methods in terms of SHD and SID, while maintaining a runtime similar to CAM. For the hundred-node data sets, the runtime of DCDI increases significantly with a SHD/SID performance comparable to the much faster GIES. We believe the weaker performance of DCDI in the hundred-node setting is due to the fact that the conditionals are high dimensional functions which are prone to overfitting. Also, we believe this runtime could be significantly reduced by limiting the number of parents via preliminary neighborhood selection similar to CAM [2]. This would have the effect of reducing the cost of computing the gradient of w.r.t. to the neural networks parameters. These adaptations to higher dimensionality are left as future work.

C.4 Ablation study

In this section, we show that the proposed losses are relevant by doing an ablation study. We also show that interventions are beneficial to recover the DAG compared to the use of observational data alone. First, in a small scale experiment, we show in Figure 11 the effect of the number of interventions on the performance of DCDI-G. The SHD and SID of DCDI-G and DCD are shown over ten linear data sets (20-node graph with sparse connectivity) with $\{0, 5, 10, 15, 20\}$ perfect interventions. The baseline DCD is equivalent to DCDI-G, but it uses a loss that doesn't take into account the interventions. It can first be noticed that, as the number of interventions increase, the performance of DCDI-G increases. This increase is particularly noticeable from the purely interventional data to data with 5 interventions. While DCD's performance also increases in term of SHD, it seems to have no clear gain in term of SID. Also, DCDI-G with interventional data is always better than DCD showing that the proposed loss for perfect interventions is pertinent. Note that the first two boxes are the same since DCDI-G on observational data is equivalent to DCD (the experiment was done only once).

In a larger scale experiment, with the same data sets used in the main text (Section 4), we compare DCDI-G and DCDI-DSF to DCD and DCD-no-interv for perfect/known, imperfect/known and perfect/unknown interventions (shown respectively in Appendix C.4.1, C.4.2, and C.4.3). The values reported are the mean and the standard deviation of SHD and SID over ten data sets of each condition. DCD-no-interv is DCDI-G applied to purely observational data. These purely observational data sets were generated from the same CGM as the other data set containing interventions and had the same total sample size. For SHD, the advantage of DCDI over DCD and DCD-no-interv is clear over all conditions. For SID, DCDI has no advantage for sparse graphs, but is usually better for graphs with higher connectivity. As in the first small scale experiment, the beneficial effect of intervention is clear. Also, these results show that the proposed losses for the different type of interventions are pertinent.

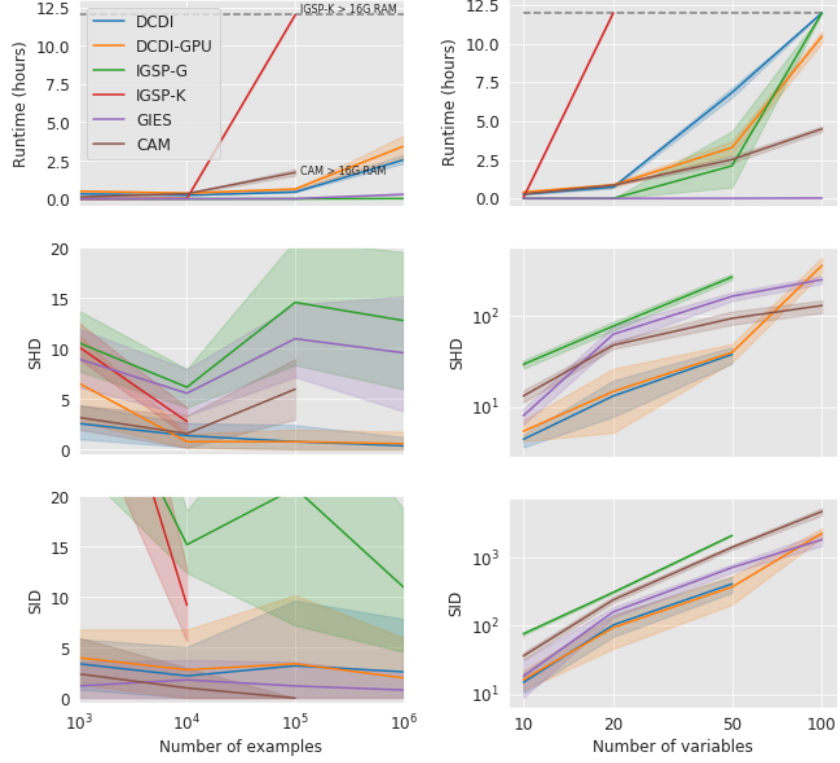


Figure 10: We report the runtime (in hours), SHD and SID of multiple methods in multiple settings. The horizontal dashed lines at 12 hours represents the time limit imposed. When a curve reaches this dashed line, it means that the method could not finish within 12 hours. We write $\geq 16G$ when the RAM memory needed by the algorithm exceeded 16GB. All data sets have 10 interventional targets containing $0.1d$ targets. We considered perfect interventions. **Left:** Different data set sizes. Ten nodes ANM data with connectivity $e = 1$. **Right:** Different number of variables. NN data set with connectivity $e = 4$ and 10^4 samples. Each curve is an average over 5 different datasets while the error bars are %95 confidence intervals computed via bootstrap.

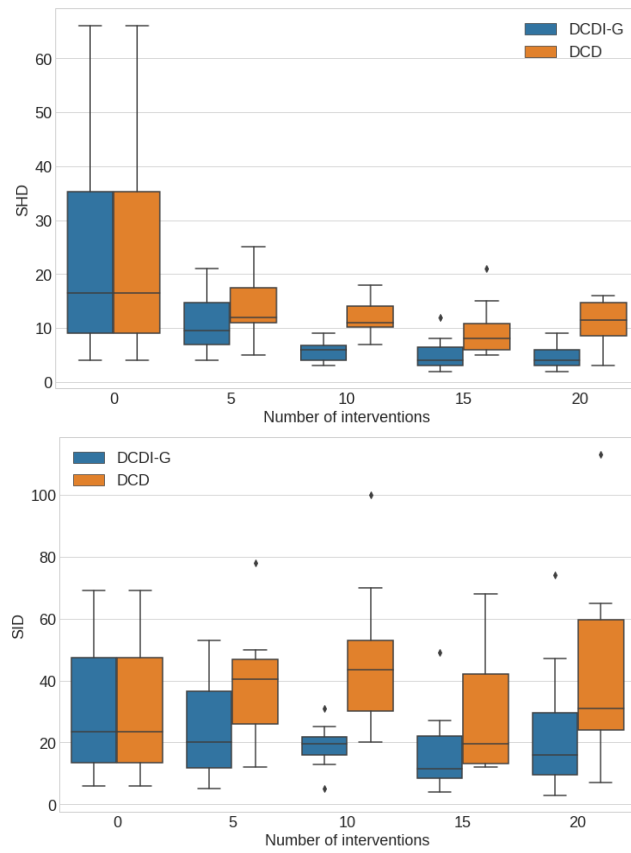


Figure 11: SHD and SID for DCDI-G and DCD on data sets with a different number of interventional settings.

C.4.1 Perfect interventions

Table 4: Results for the linear data set with perfect intervention

Method	10 nodes, $e = 1$		10 nodes, $e = 4$		20 nodes, $e = 1$		20 nodes, $e = 4$	
	SHD	SID	SHD	SID	SHD	SID	SHD	SID
DCD	6.6 \pm 3.6	14.1 \pm 11.5	24.4 \pm 6.0	67.0 \pm 9.2	18.2 \pm 15.8	30.9 \pm 21.7	56.7 \pm 10.2	227.0 \pm 38.6
DCD-no-interv	8.9 \pm 2.8	19.5 \pm 10.9	26.7 \pm 5.9	69.0 \pm 11.2	24.6 \pm 20.5	31.2 \pm 22.8	64.4 \pm 11.4	292.9 \pm 28.9
DCDI-G	1.3 \pm 1.9	0.8 \pm 1.8	3.3 \pm 2.1	10.7 \pm 12.0	5.4 \pm 4.5	13.4 \pm 12.0	23.7 \pm 5.6	112.8 \pm 41.8
DCDI-DSF	0.9 \pm 1.3	0.6 \pm 1.9	3.7 \pm 2.3	18.9 \pm 14.1	3.6 \pm 2.7	6.0 \pm 5.4	16.6 \pm 6.4	92.5 \pm 40.1

Table 5: Results for the additive noise model data set with perfect intervention

Method	10 nodes, $e = 1$		10 nodes, $e = 4$		20 nodes, $e = 1$		20 nodes, $e = 4$	
	SHD	SID	SHD	SID	SHD	SID	SHD	SID
DCD	11.5 \pm 6.6	18.2 \pm 11.8	30.4 \pm 3.8	75.5 \pm 4.6	39.3 \pm 28.4	39.8 \pm 33.3	62.7 \pm 14.2	241.0 \pm 44.8
DCD-no-interv	11.6 \pm 8.8	15.8 \pm 12.1	21.3 \pm 5.2	63.5 \pm 12.3	41.7 \pm 44.1	36.2 \pm 27.1	43.7 \pm 9.2	226.1 \pm 42.8
DCDI-G	5.2 \pm 7.5	2.4 \pm 4.9	4.3 \pm 2.4	16.0 \pm 11.9	21.8 \pm 30.1	11.6 \pm 13.1	35.2 \pm 13.2	109.8 \pm 44.6
DCDI-DSF	4.2 \pm 5.6	5.6 \pm 5.5	5.5 \pm 2.4	23.9 \pm 14.3	4.3 \pm 1.9	19.7 \pm 12.6	26.7 \pm 16.9	105.3 \pm 22.7

Table 6: Results for the nonlinear with non-additive noise data set with perfect intervention

Method	10 nodes, $e = 1$		10 nodes, $e = 4$		20 nodes, $e = 1$		20 nodes, $e = 4$	
	SHD	SID	SHD	SID	SHD	SID	SHD	SID
DCD	5.9 \pm 6.9	10.9 \pm 10.4	15.7 \pm 4.9	53.0 \pm 9.9	28.7 \pm 13.0	29.7 \pm 9.3	29.3 \pm 8.9	163.1 \pm 48.4
DCD-no-interv	11.0 \pm 9.3	9.9 \pm 11.0	18.4 \pm 6.4	56.4 \pm 11.0	16.5 \pm 22.8	31.9 \pm 17.5	31.6 \pm 11.3	160.3 \pm 46.3
DCDI-G	2.3 \pm 3.6	2.7 \pm 3.3	2.4 \pm 1.6	13.9 \pm 8.5	13.9 \pm 20.3	13.7 \pm 8.1	16.8 \pm 8.7	82.5 \pm 38.1
DCDI-DSF	7.0 \pm 10.7	7.8 \pm 5.8	1.6 \pm 1.6	7.7 \pm 13.8	8.3 \pm 4.1	32.4 \pm 17.3	11.8 \pm 2.1	102.3 \pm 34.5

C.4.2 Imperfect interventions

Table 7: Results for the linear data set with imperfect intervention

Method	10 nodes, $e = 1$		10 nodes, $e = 4$		20 nodes, $e = 1$		20 nodes, $e = 4$	
	SHD	SID	SHD	SID	SHD	SID	SHD	SID
DCD	10.6 \pm 5.4	24.6 \pm 18.2	24.0 \pm 4.1	67.2 \pm 7.6	21.2 \pm 11.5	56.0 \pm 31.5	56.7 \pm 9.0	268.0 \pm 25.4
DCD-no-interv	6.8 \pm 4.4	19.5 \pm 13.2	27.4 \pm 4.4	74.0 \pm 7.2	19.8 \pm 9.2	48.2 \pm 30.6	58.2 \pm 9.9	288.6 \pm 31.6
DCDI-G	2.7 \pm 2.8	8.2 \pm 8.8	5.2 \pm 3.5	25.1 \pm 12.9	15.6 \pm 14.5	29.1 \pm 23.4	34.0 \pm 7.7	180.9 \pm 44.5
DCDI-DSF	1.3 \pm 1.3	4.2 \pm 4.0	1.7 \pm 2.4	10.2 \pm 14.9	6.9 \pm 6.3	22.7 \pm 21.9	21.7 \pm 8.1	137.4 \pm 34.3

Table 8: Results for the additive noise model data set with imperfect intervention

Method	10 nodes, $e = 1$		10 nodes, $e = 4$		20 nodes, $e = 1$		20 nodes, $e = 4$	
	SHD	SID	SHD	SID	SHD	SID	SHD	SID
DCD	12.0 \pm 9.2	14.8 \pm 10.4	24.3 \pm 3.8	64.5 \pm 11.1	51.7 \pm 41.7	44.5 \pm 20.0	54.1 \pm 12.0	196.6 \pm 37.2
DCD-no-interv	14.6 \pm 4.3	12.1 \pm 11.8	24.8 \pm 4.8	69.3 \pm 8.3	49.5 \pm 36.0	32.7 \pm 22.7	41.2 \pm 8.1	197.7 \pm 50.1
DCDI-G	6.2 \pm 5.4	7.6 \pm 11.0	13.1 \pm 2.9	48.1 \pm 9.1	30.5 \pm 33.0	12.5 \pm 8.8	43.1 \pm 10.2	96.6 \pm 47.1
DCDI-DSF	13.4 \pm 8.4	17.9 \pm 10.5	14.4 \pm 2.4	53.2 \pm 8.2	13.1 \pm 4.5	43.5 \pm 19.2	50.5 \pm 11.4	172.1 \pm 19.6

Table 9: Results for the nonlinear with non-additive noise data set with imperfect intervention

Method	10 nodes, $e = 1$		10 nodes, $e = 4$		20 nodes, $e = 1$		20 nodes, $e = 4$	
	SHD	SID	SHD	SID	SHD	SID	SHD	SID
DCD	12.7 \pm 8.4	11.8 \pm 7.3	15.2 \pm 3.7	52.2 \pm 9.1	40.4 \pm 54.7	45.2 \pm 43.9	30.5 \pm 8.0	151.2 \pm 41.7
DCD-no-interv	13.6 \pm 9.7	13.0 \pm 8.1	14.8 \pm 3.5	51.7 \pm 12.5	37.1 \pm 40.7	57.1 \pm 56.2	31.3 \pm 5.5	162.3 \pm 40.5
DCDI-G	3.9 \pm 3.9	7.5 \pm 6.5	7.3 \pm 2.2	28.0 \pm 10.5	18.2 \pm 28.8	36.9 \pm 37.0	21.7 \pm 8.0	127.3 \pm 40.1
DCDI-DSF	5.3 \pm 4.2	16.3 \pm 10.0	5.9 \pm 3.2	35.1 \pm 12.3	13.2 \pm 5.1	76.5 \pm 57.8	16.8 \pm 5.3	143.6 \pm 48.8

C.4.3 Unknown interventions

Table 10: Results for the linear data set with perfect intervention with unknown targets

Method	10 nodes, $e = 1$		10 nodes, $e = 4$		20 nodes, $e = 1$		20 nodes, $e = 4$	
	SHD	SID	SHD	SID	SHD	SID	SHD	SID
DCD	6.6 \pm 3.6	14.1 \pm 11.5	24.4 \pm 6.0	67.0 \pm 9.2	18.2 \pm 15.8	30.9 \pm 21.7	56.7 \pm 10.2	227.0 \pm 38.6
DCD-no-interv	8.9 \pm 2.8	19.5 \pm 10.9	26.7 \pm 5.9	69.0 \pm 11.2	24.6 \pm 20.5	31.2 \pm 22.8	64.4 \pm 11.4	292.9 \pm 28.9
DCDI-G	5.3 \pm 3.7	12.9 \pm 11.5	5.2 \pm 3.0	24.3 \pm 15.3	15.4 \pm 10.3	30.8 \pm 18.6	39.2 \pm 8.7	173.7 \pm 45.6
DCDI-DSF	3.9 \pm 4.3	7.1 \pm 7.1	7.1 \pm 3.6	35.8 \pm 12.5	4.3 \pm 2.4	18.4 \pm 7.3	29.7 \pm 12.6	147.8 \pm 42.7

Table 11: Results for the additive noise model data set with perfect intervention with unknown targets

Method	10 nodes, $e = 1$		10 nodes, $e = 4$		20 nodes, $e = 1$		20 nodes, $e = 4$	
	SHD	SID	SHD	SID	SHD	SID	SHD	SID
DCD	11.5 \pm 6.6	18.2 \pm 11.8	30.4 \pm 3.8	75.5 \pm 4.6	39.3 \pm 28.4	39.8 \pm 33.3	62.7 \pm 14.2	241.0 \pm 44.8
DCD-no-interv	11.6 \pm 8.8	15.8 \pm 12.1	21.3 \pm 5.2	63.5 \pm 12.3	41.7 \pm 44.1	36.2 \pm 27.1	43.7 \pm 9.2	226.1 \pm 42.8
DCDI-G	7.6 \pm 10.3	5.0 \pm 5.4	9.1 \pm 3.8	37.5 \pm 14.1	41.3 \pm 39.2	22.9 \pm 15.5	39.9 \pm 18.8	153.7 \pm 50.3
DCDI-DSF	11.9 \pm 8.8	13.8 \pm 7.9	6.6 \pm 2.6	32.6 \pm 14.1	22.3 \pm 31.9	33.1 \pm 17.5	42.5 \pm 18.7	152.9 \pm 53.4

Table 12: Results for the nonlinear with non-additive noise data set with perfect intervention with unknown targets

Method	10 nodes, $e = 1$		10 nodes, $e = 4$		20 nodes, $e = 1$		20 nodes, $e = 4$	
	SHD	SID	SHD	SID	SHD	SID	SHD	SID
DCD	5.9 \pm 6.9	10.9 \pm 10.4	15.7 \pm 4.9	53.0 \pm 9.9	28.7 \pm 13.0	29.7 \pm 9.3	29.3 \pm 8.9	163.1 \pm 48.4
DCD-no-interv	11.0 \pm 9.3	9.9 \pm 11.0	18.4 \pm 6.4	56.4 \pm 11.0	16.5 \pm 22.8	31.9 \pm 17.5	31.6 \pm 11.3	160.3 \pm 46.3
DCDI-G	3.4 \pm 4.2	6.9 \pm 7.5	3.3 \pm 1.3	20.4 \pm 10.4	21.8 \pm 32.1	20.9 \pm 12.3	20.1 \pm 8.1	104.6 \pm 47.1
DCDI-DSF	7.8 \pm 7.9	11.8 \pm 5.7	3.3 \pm 1.2	23.2 \pm 9.1	27.4 \pm 30.9	49.3 \pm 15.7	22.2 \pm 10.4	131.0 \pm 41.0

C.5 Different kinds of interventions

In this section, we compare DCDI to IGSP using data sets under different kinds of interventions. We report results in tabular form for 10-node and 20-node graphs. For the perfect interventions, instead of replacing the target conditional distribution by the marginal $\mathcal{N}(2, 1)$ (as in the main results), we used a marginal that doesn't involve a mean-shift: $\mathcal{U}[-1, 1]$. The results reported in Tables 13, 14, 15 of Section C.5.1 are the mean and the standard deviation of SHD and SID over ten data sets of each condition. From these results, we can conclude that DCDI-G still outperforms IGSP and, by comparing to DCD (DCDI-G with a loss that doesn't take into account interventions), that the proposed loss is still beneficial for this kind of interventions. It has competitive results compared to GIES and CAM on the linear data set and it outperforms them on the other data sets.

For imperfect intervention, we tried more modest changes in the parameters. For the linear data set, an imperfect intervention consisted of adding $\mathcal{U}[0.5, 1]$ to w_j if $w_j > 0$ and subtracting if $w_j \leq 0$. It was done this way to ensure that the intervention would not remove dependencies between variables. For the additive noise model and the nonlinear with non-additive noise data sets, $\mathcal{N}(0, 0.1)$ was added to each weight of the neural networks. Results are reported in Tables 16, 17, 18 of Section C.5.2. These smaller changes made the difference between DCD and DCDI imperceptible. For sparse

graphs, IGSP has a better or comparable performance to DCDI. For graphs with higher connectivity, DCDI often has a better performance than IGSP.

C.5.1 Perfect interventions

Table 13: Results for the linear data set with perfect intervention

Method	10 nodes, $e = 1$		10 nodes, $e = 4$		20 nodes, $e = 1$		20 nodes, $e = 4$	
	SHD	SID	SHD	SID	SHD	SID	SHD	SID
IGSP	4.0 ± 4.8	15.7 ± 15.4	28.8 ± 2.0	72.2 ± 5.1	9.7 ± 8.7	45.1 ± 45.4	68.1 ± 13.6	295.4 ± 27.6
GIES	0.3 ± 0.5	0.0 ± 0.0	4.0 ± 6.5	6.7 ± 17.7	1.5 ± 1.2	0.3 ± 0.9	49.4 ± 22.2	111.9 ± 51.4
CAM	0.6 ± 1.0	0.0 ± 0.0	11.8 ± 4.3	32.2 ± 17.2	6.3 ± 7.4	7.6 ± 9.8	91.4 ± 21.3	181.7 ± 60.5
DCD	6.3 ± 3.4	14.8 ± 10.6	26.1 ± 3.3	66.4 ± 11.4	11.1 ± 4.7	45.8 ± 22.8	49.0 ± 12.0	258.6 ± 41.6
DCDI-G	0.4 ± 0.7	1.3 ± 2.1	7.5 ± 1.4	29.7 ± 8.2	3.2 ± 3.2	12.1 ± 11.2	21.0 ± 4.9	147.6 ± 49.5

Table 14: Results for the additive noise model data set with perfect intervention

Method	10 nodes, $e = 1$		10 nodes, $e = 4$		20 nodes, $e = 1$		20 nodes, $e = 4$	
	SHD	SID	SHD	SID	SHD	SID	SHD	SID
IGSP	5.7 ± 2.3	23.4 ± 13.6	32.8 ± 2.4	79.3 ± 3.2	14.9 ± 8.1	78.8 ± 64.6	80.5 ± 6.4	337.6 ± 27.3
GIES	7.5 ± 5.1	2.3 ± 2.5	9.2 ± 2.9	27.1 ± 11.5	23.8 ± 18.4	3.1 ± 4.4	89.6 ± 14.7	143.9 ± 53.1
CAM	6.3 ± 6.9	0.0 ± 0.0	6.3 ± 3.8	14.6 ± 20.1	9.2 ± 14.3	13.5 ± 25.1	106.2 ± 14.6	96.2 ± 57.9
DCD	6.4 ± 4.6	22.0 ± 14.7	31.1 ± 3.4	77.4 ± 3.1	18.1 ± 8.0	51.5 ± 41.5	55.7 ± 8.3	261.3 ± 22.5
DCDI-G	0.9 ± 1.2	3.9 ± 6.4	5.2 ± 1.9	24.0 ± 9.3	6.5 ± 5.6	17.9 ± 19.1	26.8 ± 7.0	94.4 ± 41.5

Table 15: Results for the nonlinear with non-additive noise data set with perfect intervention

Method	10 nodes, $e = 1$		10 nodes, $e = 4$		20 nodes, $e = 1$		20 nodes, $e = 4$	
	SHD	SID	SHD	SID	SHD	SID	SHD	SID
IGSP	6.6 ± 3.9	25.8 ± 17.9	31.1 ± 3.3	77.1 ± 5.7	14.4 ± 4.8	63.8 ± 26.5	79.7 ± 8.1	341.4 ± 18.1
GIES	6.2 ± 3.5	0.9 ± 1.5	9.5 ± 3.6	29.0 ± 17.7	12.2 ± 2.1	3.4 ± 3.2	63.8 ± 11.1	124.9 ± 36.9
CAM	4.1 ± 3.8	2.3 ± 3.4	11.3 ± 4.2	35.4 ± 20.8	4.2 ± 2.3	10.9 ± 10.3	106.6 ± 15.7	144.2 ± 51.8
DCD	6.6 ± 3.5	18.1 ± 8.1	20.6 ± 3.9	65.8 ± 9.9	9.4 ± 4.9	25.6 ± 16.2	28.6 ± 6.8	188.0 ± 28.7
DCDI-G	2.1 ± 1.5	4.6 ± 5.4	5.0 ± 4.3	28.8 ± 17.6	6.4 ± 3.8	15.1 ± 8.0	12.2 ± 2.7	96.1 ± 18.9

C.5.2 Imperfect interventions

Table 16: Results for the linear data set with imperfect intervention

Method	10 nodes, $e = 1$		10 nodes, $e = 4$		20 nodes, $e = 1$		20 nodes, $e = 4$	
	SHD	SID	SHD	SID	SHD	SID	SHD	SID
IGSP	1.1 ± 1.1	5.4 ± 5.4	28.7 ± 3.2	72.4 ± 6.7	4.2 ± 3.9	17.7 ± 12.3	86.1 ± 12.3	289.8 ± 26.3
DCD	3.8 ± 3.6	9.4 ± 6.4	27.7 ± 3.4	74.6 ± 3.5	27.2 ± 22.3	39.3 ± 20.5	65.0 ± 8.0	306.8 ± 26.3
DCDI-G	4.7 ± 4.5	11.5 ± 9.5	27.4 ± 4.9	73.8 ± 5.4	29.6 ± 16.5	37.7 ± 14.5	62.8 ± 6.5	303.2 ± 27.6
DCDI-DSF	4.1 ± 2.3	10.3 ± 7.5	24.3 ± 5.3	69.1 ± 8.7	12.2 ± 2.9	42.6 ± 18.3	56.1 ± 9.2	291.4 ± 35.7

Table 17: Results for the additive noise model data set with imperfect intervention

Method	10 nodes, $e = 1$		10 nodes, $e = 4$		20 nodes, $e = 1$		20 nodes, $e = 4$	
	SHD	SID	SHD	SID	SHD	SID	SHD	SID
IGSP	5.7 ± 4.0	17.4 ± 13.4	30.3 ± 4.0	73.9 ± 11.3	12.5 ± 6.6	44.9 ± 26.7	85.8 ± 4.4	344.0 ± 9.8
DCD	12.0 ± 10.3	11.3 ± 8.4	23.5 ± 2.1	69.7 ± 2.5	39.5 ± 42.3	28.2 ± 13.9	50.9 ± 7.1	247.8 ± 36.6
DCDI-G	12.7 ± 9.1	11.8 ± 6.5	21.7 ± 4.3	65.2 ± 9.2	16.2 ± 18.0	27.8 ± 13.1	46.2 ± 5.9	240.1 ± 26.3
DCDI-DSF	8.1 ± 8.2	15.8 ± 9.3	23.3 ± 6.3	68.7 ± 8.2	12.3 ± 4.1	39.9 ± 19.5	51.0 ± 7.1	257.7 ± 31.6

Table 18: Results for the nonlinear with non-additive noise data set with imperfect intervention

Method	10 nodes, $e = 1$		10 nodes, $e = 4$		20 nodes, $e = 1$		20 nodes, $e = 4$	
	SHD	SID	SHD	SID	SHD	SID	SHD	SID
IGSP	7.0 ± 5.7	22.7 ± 19.5	29.4 ± 5.0	74.2 ± 7.3	18.7 ± 7.1	86.3 ± 37.1	81.6 ± 6.9	344.4 ± 20.5
DCD	9.4 ± 8.9	13.3 ± 11.0	15.1 ± 3.7	54.2 ± 9.8	28.5 ± 25.0	25.5 ± 16.8	32.7 ± 9.8	177.1 ± 37.5
DCDI-G	6.7 ± 5.1	13.0 ± 9.7	14.6 ± 3.3	53.9 ± 9.1	28.9 ± 33.7	25.2 ± 15.2	32.3 ± 7.9	177.0 ± 55.8
DCDI-DSF	12.8 ± 9.6	22.9 ± 14.8	14.4 ± 4.8	54.2 ± 10.3	13.3 ± 5.3	54.2 ± 20.9	28.6 ± 8.9	199.5 ± 32.7

C.6 Comprehensive results of the main experiments

In this section, we report the main results presented in Section 4 in tabular form for 10-node and 20-node graphs. We also include additional results for different cutoff values for IGSP and UT-IGSP, namely $\log_{10} \alpha = \{-2, -3, -5, -7, -9\}$. This range was chosen to be around the cutoff value of 10^{-5} used in [34]. The reported values in the following tables are the mean and the standard deviation of SHD and SID over ten data sets of each condition. As stated in the main discussion, our conclusions are similar for 10-node graphs: DCDI has competitive performance in all conditions and outperforms the other methods for graphs with higher connectivity.

C.6.1 Perfect interventions

Table 19: Results for linear data set with perfect intervention

Method	10 nodes, $e = 1$		10 nodes, $e = 4$		20 nodes, $e = 1$		20 nodes, $e = 4$	
	SHD	SID	SHD	SID	SHD	SID	SHD	SID
IGSP($\alpha=1e-2$)	2.4 ± 2.0	9.9 ± 9.5	27.4 ± 4.2	71.1 ± 6.1	6.1 ± 5.1	18.2 ± 11.8	74.7 ± 15.9	272.4 ± 33.7
IGSP($\alpha=1e-3$)	2.4 ± 2.2	10.3 ± 10.4	29.4 ± 3.7	73.8 ± 8.1	8.3 ± 6.7	32.1 ± 35.4	79.6 ± 12.4	298.1 ± 16.7
IGSP($\alpha=1e-5$)	2.4 ± 2.2	10.9 ± 10.5	31.6 ± 3.8	75.7 ± 5.8	9.4 ± 5.1	39.3 ± 33.6	84.3 ± 10.5	324.7 ± 12.3
IGSP($\alpha=1e-7$)	2.6 ± 2.5	13.4 ± 14.6	33.2 ± 3.1	79.6 ± 3.4	9.0 ± 5.5	46.0 ± 39.1	81.7 ± 7.6	336.5 ± 16.6
IGSP($\alpha=1e-9$)	2.5 ± 2.3	12.6 ± 12.9	29.6 ± 2.9	73.1 ± 6.7	12.2 ± 5.1	64.9 ± 44.1	82.8 ± 6.4	341.5 ± 14.2
GIES	0.7 ± 1.1	0.0 ± 0.0	4.7 ± 3.7	6.5 ± 13.9	1.1 ± 1.2	0.0 ± 0.0	52.8 ± 18.9	79.8 ± 68.3
CAM	1.9 ± 2.6	1.7 ± 3.1	10.6 ± 3.1	34.5 ± 11.0	5.4 ± 7.9	8.2 ± 9.6	91.1 ± 21.7	167.8 ± 55.4
DCDI-G	1.3 ± 1.9	0.8 ± 1.8	3.3 ± 2.1	10.7 ± 12.0	5.4 ± 4.5	13.4 ± 12.0	23.7 ± 5.6	112.8 ± 41.8
DCDI-DSF	0.9 ± 1.3	0.6 ± 1.9	3.7 ± 2.3	18.9 ± 14.1	3.6 ± 2.7	6.0 ± 5.4	16.6 ± 6.4	92.5 ± 40.1

Table 20: Results for the additive noise model data set with perfect intervention

Method	10 nodes, $e = 1$		10 nodes, $e = 4$		20 nodes, $e = 1$		20 nodes, $e = 4$	
	SHD	SID	SHD	SID	SHD	SID	SHD	SID
IGSP($\alpha=1e-2$)	7.7 ± 3.5	21.6 ± 11.3	31.3 ± 2.5	79.7 ± 3.0	18.4 ± 6.5	77.6 ± 41.6	83.9 ± 9.6	323.0 ± 13.6
IGSP($\alpha=1e-3$)	9.0 ± 3.9	27.9 ± 15.2	30.1 ± 3.9	77.6 ± 4.9	16.9 ± 8.8	79.5 ± 54.2	83.8 ± 8.9	335.0 ± 21.7
IGSP($\alpha=1e-5$)	8.0 ± 3.8	30.1 ± 14.9	31.4 ± 4.2	79.3 ± 4.2	16.6 ± 6.5	80.0 ± 50.8	80.6 ± 8.3	325.5 ± 24.3
IGSP($\alpha=1e-7$)	8.3 ± 4.3	33.1 ± 15.0	33.2 ± 2.5	78.4 ± 6.3	16.3 ± 6.9	81.3 ± 48.9	81.3 ± 6.1	330.0 ± 25.5
IGSP($\alpha=1e-9$)	9.5 ± 5.2	33.5 ± 13.0	31.3 ± 5.1	72.7 ± 11.9	15.5 ± 6.7	78.8 ± 51.4	80.6 ± 10.2	335.4 ± 17.1
GIES	7.6 ± 4.6	1.9 ± 2.9	10.5 ± 2.5	24.6 ± 13.8	24.2 ± 12.4	7.5 ± 13.8	94.4 ± 10.9	144.4 ± 62.0
CAM	5.2 ± 3.0	1.0 ± 1.9	8.5 ± 3.7	11.5 ± 13.4	7.5 ± 6.0	5.6 ± 4.9	105.7 ± 13.2	108.7 ± 61.0
DCDI-G	5.2 ± 7.5	2.4 ± 4.9	4.3 ± 2.4	16.0 ± 11.9	21.8 ± 30.1	11.6 ± 13.1	35.2 ± 13.2	109.8 ± 44.6
DCDI-DSF	4.2 ± 5.6	5.6 ± 5.5	5.5 ± 2.4	23.9 ± 14.3	4.3 ± 1.9	19.7 ± 12.6	26.7 ± 16.9	105.3 ± 22.7

Table 21: Results for the nonlinear with non-additive noise data set with perfect intervention

Method	10 nodes, $e = 1$		10 nodes, $e = 4$		20 nodes, $e = 1$		20 nodes, $e = 4$	
	SHD	SID	SHD	SID	SHD	SID	SHD	SID
IGSP($\alpha=1e-2$)	5.4 \pm 3.1	13.7 \pm 6.4	29.8 \pm 4.0	73.0 \pm 8.4	19.6 \pm 3.9	80.5 \pm 22.7	81.8 \pm 8.7	336.2 \pm 18.0
IGSP($\alpha=1e-3$)	5.7 \pm 2.9	19.4 \pm 13.0	30.4 \pm 3.3	73.5 \pm 10.8	17.9 \pm 5.6	85.6 \pm 37.1	80.6 \pm 11.9	330.7 \pm 23.5
IGSP($\alpha=1e-5$)	6.1 \pm 3.0	19.5 \pm 12.1	33.3 \pm 3.7	78.6 \pm 5.2	19.6 \pm 4.5	94.4 \pm 30.2	77.0 \pm 9.5	345.2 \pm 9.8
IGSP($\alpha=1e-7$)	6.4 \pm 3.0	22.6 \pm 13.1	33.8 \pm 3.4	77.4 \pm 10.1	18.5 \pm 4.0	85.9 \pm 29.1	76.1 \pm 11.3	347.5 \pm 15.9
IGSP($\alpha=1e-9$)	6.7 \pm 3.7	24.8 \pm 15.9	34.9 \pm 2.7	78.8 \pm 9.1	19.5 \pm 4.6	100.6 \pm 33.5	77.9 \pm 9.2	341.9 \pm 24.6
GIES	4.0 \pm 2.4	0.8 \pm 1.3	8.3 \pm 3.1	26.5 \pm 12.2	13.9 \pm 5.7	9.4 \pm 9.4	65.9 \pm 16.5	110.6 \pm 48.9
CAM	1.8 \pm 1.5	2.8 \pm 4.4	7.9 \pm 3.6	26.7 \pm 19.0	6.1 \pm 5.2	18.1 \pm 16.3	101.8 \pm 24.5	142.5 \pm 49.1
DCDI-G	2.3 \pm 3.6	2.7 \pm 3.3	2.4 \pm 1.6	13.9 \pm 8.5	13.9 \pm 20.3	13.7 \pm 8.1	16.8 \pm 8.7	82.5 \pm 38.1
DCDI-DSF	7.0 \pm 10.7	7.8 \pm 5.8	1.6 \pm 1.6	7.7 \pm 13.8	8.3 \pm 4.1	32.4 \pm 17.3	11.8 \pm 2.1	102.3 \pm 34.5

C.6.2 Imperfect interventions

Table 22: Results for the linear data set with imperfect intervention

Method	10 nodes, $e = 1$		10 nodes, $e = 4$		20 nodes, $e = 1$		20 nodes, $e = 4$	
	SHD	SID	SHD	SID	SHD	SID	SHD	SID
IGSP($\alpha=1e-2$)	2.1 \pm 1.0	10.8 \pm 8.1	27.2 \pm 5.5	71.7 \pm 6.8	6.6 \pm 4.0	20.8 \pm 14.2	64.0 \pm 9.3	271.0 \pm 24.7
IGSP($\alpha=1e-3$)	3.4 \pm 2.8	15.9 \pm 9.5	28.3 \pm 6.1	74.6 \pm 7.2	6.1 \pm 4.6	30.1 \pm 22.8	74.1 \pm 14.4	298.5 \pm 21.0
IGSP($\alpha=1e-5$)	3.4 \pm 2.4	17.0 \pm 13.1	30.3 \pm 3.2	76.1 \pm 5.9	7.9 \pm 5.2	44.5 \pm 37.8	77.8 \pm 11.2	324.2 \pm 17.8
IGSP($\alpha=1e-7$)	3.8 \pm 1.5	18.4 \pm 8.8	29.4 \pm 3.4	76.5 \pm 5.1	10.9 \pm 5.5	56.7 \pm 30.5	78.0 \pm 8.6	333.1 \pm 17.1
IGSP($\alpha=1e-9$)	5.1 \pm 3.2	24.5 \pm 18.8	31.8 \pm 3.1	79.7 \pm 4.9	11.2 \pm 5.6	62.4 \pm 34.1	75.2 \pm 9.2	341.6 \pm 24.2
GIES	5.8 \pm 5.4	20.3 \pm 19.2	10.8 \pm 6.6	38.7 \pm 23.0	4.9 \pm 3.8	22.2 \pm 23.9	81.5 \pm 18.8	200.4 \pm 50.3
CAM	8.1 \pm 6.2	22.6 \pm 18.8	19.4 \pm 4.7	56.0 \pm 10.1	10.5 \pm 5.8	36.3 \pm 23.6	111.7 \pm 16.5	232.5 \pm 23.4
DCDI-G	2.7 \pm 2.8	8.2 \pm 8.8	5.2 \pm 3.5	25.1 \pm 12.9	15.6 \pm 14.5	29.1 \pm 23.4	34.0 \pm 7.7	180.9 \pm 44.5
DCDI-DSF	1.3 \pm 1.3	4.2 \pm 4.0	1.7 \pm 2.4	10.2 \pm 14.9	6.9 \pm 6.3	22.7 \pm 21.9	21.7 \pm 8.1	137.4 \pm 34.3

Table 23: Results for the additive noise model data set with imperfect intervention

Method	10 nodes, $e = 1$		10 nodes, $e = 4$		20 nodes, $e = 1$		20 nodes, $e = 4$	
	SHD	SID	SHD	SID	SHD	SID	SHD	SID
IGSP($\alpha=1e-2$)	9.2 \pm 5.2	22.4 \pm 11.3	34.0 \pm 4.0	77.4 \pm 4.5	20.9 \pm 6.8	83.8 \pm 38.6	84.7 \pm 6.4	328.2 \pm 16.2
IGSP($\alpha=1e-3$)	9.0 \pm 4.8	27.5 \pm 12.4	33.0 \pm 2.5	80.5 \pm 2.4	19.7 \pm 4.7	85.4 \pm 34.8	82.6 \pm 5.4	330.9 \pm 19.0
IGSP($\alpha=1e-5$)	7.9 \pm 3.5	26.9 \pm 15.1	34.8 \pm 3.0	81.2 \pm 3.7	20.6 \pm 4.6	92.8 \pm 46.7	84.7 \pm 8.2	338.4 \pm 16.1
IGSP($\alpha=1e-7$)	7.8 \pm 3.5	25.0 \pm 13.6	34.2 \pm 2.3	82.0 \pm 1.9	19.2 \pm 4.7	82.8 \pm 30.1	84.8 \pm 6.7	340.2 \pm 25.8
IGSP($\alpha=1e-9$)	7.9 \pm 3.7	24.7 \pm 13.9	34.5 \pm 3.1	81.2 \pm 3.7	19.4 \pm 2.9	91.2 \pm 27.1	80.3 \pm 6.4	335.7 \pm 23.5
GIES	17.6 \pm 6.7	24.6 \pm 12.9	18.1 \pm 5.1	58.0 \pm 9.0	35.3 \pm 17.1	55.4 \pm 41.3	121.2 \pm 12.4	236.5 \pm 29.1
CAM	11.2 \pm 9.3	7.8 \pm 8.7	9.6 \pm 3.0	25.2 \pm 10.8	16.3 \pm 9.9	26.7 \pm 27.2	121.9 \pm 11.6	155.4 \pm 41.5
DCDI-G	6.2 \pm 5.4	7.6 \pm 11.0	13.1 \pm 2.9	48.1 \pm 9.1	30.5 \pm 33.0	12.5 \pm 8.8	43.1 \pm 10.2	96.6 \pm 47.1
DCDI-DSF	13.4 \pm 8.4	17.9 \pm 10.5	14.4 \pm 2.4	53.2 \pm 8.2	13.1 \pm 4.5	43.5 \pm 19.2	50.5 \pm 11.4	172.1 \pm 19.6

Table 24: Results for the nonlinear with non-additive noise data set with imperfect intervention

Method	10 nodes, $e = 1$		10 nodes, $e = 4$		20 nodes, $e = 1$		20 nodes, $e = 4$	
	SHD	SID	SHD	SID	SHD	SID	SHD	SID
IGSP($\alpha=1e-2$)	7.0 \pm 4.5	24.3 \pm 19.0	30.0 \pm 4.1	76.1 \pm 5.5	21.9 \pm 8.9	103.2 \pm 77.7	79.0 \pm 8.6	335.5 \pm 20.5
IGSP($\alpha=1e-3$)	6.4 \pm 5.0	27.0 \pm 20.9	30.1 \pm 4.8	74.4 \pm 7.0	20.9 \pm 7.0	115.9 \pm 78.6	76.5 \pm 7.8	344.1 \pm 21.8
IGSP($\alpha=1e-5$)	5.8 \pm 5.0	22.6 \pm 20.6	30.6 \pm 3.2	77.1 \pm 3.7	20.1 \pm 8.5	125.9 \pm 95.9	74.1 \pm 5.5	335.8 \pm 24.3
IGSP($\alpha=1e-7$)	6.6 \pm 4.9	22.4 \pm 17.6	32.7 \pm 3.8	78.1 \pm 5.3	20.7 \pm 8.7	124.5 \pm 82.3	76.3 \pm 5.7	340.8 \pm 25.8
IGSP($\alpha=1e-9$)	6.4 \pm 4.2	24.5 \pm 19.1	34.1 \pm 2.4	77.2 \pm 6.6	20.9 \pm 8.6	131.1 \pm 93.0	76.0 \pm 5.1	348.3 \pm 18.4
GIES	9.4 \pm 5.8	16.7 \pm 11.9	18.3 \pm 6.4	52.1 \pm 15.5	32.8 \pm 14.1	58.5 \pm 45.5	81.5 \pm 13.9	217.3 \pm 33.9
CAM	4.3 \pm 3.3	9.3 \pm 6.8	14.7 \pm 5.1	45.7 \pm 14.9	20.7 \pm 16.2	53.9 \pm 32.9	121.5 \pm 9.3	194.1 \pm 40.3
DCDI-G	3.9 \pm 3.9	7.5 \pm 6.5	7.3 \pm 2.2	28.0 \pm 10.5	18.2 \pm 28.8	36.9 \pm 37.0	21.7 \pm 8.0	127.3 \pm 40.1
DCDI-DSF	5.3 \pm 4.2	16.3 \pm 10.0	5.9 \pm 3.2	35.1 \pm 12.3	13.2 \pm 5.1	76.5 \pm 57.8	16.8 \pm 5.3	143.6 \pm 48.8

C.6.3 Unknown interventions

Table 25: Results for the linear data set with perfect intervention with unknown targets

Method	10 nodes, $e = 1$		10 nodes, $e = 4$		20 nodes, $e = 1$		20 nodes, $e = 4$	
	SHD	SID	SHD	SID	SHD	SID	SHD	SID
UTIGSP($\alpha=1e-2$)	1.7 ± 2.1	7.0 ± 9.3	27.2 ± 5.8	70.1 ± 9.8	4.7 ± 3.9	14.4 ± 10.8	69.8 ± 12.4	271.8 ± 20.8
UTIGSP($\alpha=1e-3$)	1.6 ± 2.2	7.2 ± 10.1	29.6 ± 5.5	73.1 ± 9.4	6.9 ± 6.7	25.2 ± 32.0	81.3 ± 12.4	300.7 ± 17.5
UTIGSP($\alpha=1e-5$)	1.2 ± 1.9	5.1 ± 8.7	29.4 ± 4.2	73.2 ± 7.1	8.6 ± 6.0	36.4 ± 29.9	81.5 ± 11.7	323.9 ± 14.1
UTIGSP($\alpha=1e-7$)	1.8 ± 2.6	7.6 ± 13.4	29.4 ± 3.4	72.3 ± 9.6	8.6 ± 5.6	42.5 ± 40.2	84.8 ± 9.7	339.7 ± 11.7
UTIGSP($\alpha=1e-9$)	1.8 ± 2.4	7.8 ± 13.5	29.2 ± 3.8	70.2 ± 7.5	11.6 ± 7.3	56.3 ± 48.6	81.0 ± 5.4	336.0 ± 13.6
DCDI-G	5.3 ± 3.7	12.9 ± 11.5	5.2 ± 3.0	24.3 ± 15.3	15.4 ± 10.3	30.8 ± 18.6	39.2 ± 8.7	173.7 ± 45.6
DCDI-DSF	3.9 ± 4.3	7.1 ± 7.1	7.1 ± 3.6	35.8 ± 12.5	4.3 ± 2.4	18.4 ± 7.3	29.7 ± 12.6	147.8 ± 42.7

Table 26: Results for the additive noise model data set with perfect intervention with unknown targets

Method	10 nodes, $e = 1$		10 nodes, $e = 4$		20 nodes, $e = 1$		20 nodes, $e = 4$	
	SHD	SID	SHD	SID	SHD	SID	SHD	SID
UTIGSP($\alpha=1e-2$)	9.1 ± 4.2	25.3 ± 10.3	29.0 ± 2.6	73.1 ± 3.1	19.2 ± 7.8	77.4 ± 50.9	84.9 ± 10.1	332.3 ± 14.2
UTIGSP($\alpha=1e-3$)	10.4 ± 4.1	28.1 ± 12.9	30.5 ± 4.7	77.8 ± 5.4	18.6 ± 8.5	81.4 ± 53.6	83.8 ± 5.5	331.9 ± 27.3
UTIGSP($\alpha=1e-5$)	9.9 ± 4.3	33.6 ± 12.0	32.1 ± 3.9	77.4 ± 6.7	18.7 ± 4.9	86.4 ± 41.8	83.5 ± 6.8	341.7 ± 12.4
UTIGSP($\alpha=1e-7$)	9.4 ± 4.9	33.3 ± 14.4	33.7 ± 3.9	76.8 ± 9.4	18.3 ± 6.8	84.3 ± 47.0	83.3 ± 8.1	336.8 ± 21.3
UTIGSP($\alpha=1e-9$)	9.4 ± 5.2	32.1 ± 15.2	33.0 ± 4.2	77.7 ± 8.7	18.8 ± 7.0	97.1 ± 55.9	82.9 ± 7.0	329.4 ± 28.2
DCDI-G	7.6 ± 10.3	5.0 ± 5.4	9.1 ± 3.8	37.5 ± 14.1	41.3 ± 39.2	22.9 ± 15.5	39.9 ± 18.8	153.7 ± 50.3
DCDI-DSF	11.9 ± 8.8	13.8 ± 7.9	6.6 ± 2.6	32.6 ± 14.1	22.3 ± 31.9	33.1 ± 17.5	42.5 ± 18.7	152.9 ± 53.4

Table 27: Results for the nonlinear with non-additive noise data set with perfect intervention with unknown targets

Method	10 nodes, $e = 1$		10 nodes, $e = 4$		20 nodes, $e = 1$		20 nodes, $e = 4$	
	SHD	SID	SHD	SID	SHD	SID	SHD	SID
UTIGSP($\alpha=1e-2$)	6.1 ± 4.1	16.6 ± 12.5	28.1 ± 4.8	68.4 ± 14.3	22.1 ± 5.5	100.6 ± 30.1	85.4 ± 9.1	330.0 ± 19.6
UTIGSP($\alpha=1e-3$)	6.4 ± 3.6	19.5 ± 14.5	31.0 ± 3.1	76.8 ± 4.3	20.0 ± 4.3	92.2 ± 21.6	81.1 ± 6.2	338.5 ± 10.8
UTIGSP($\alpha=1e-5$)	6.8 ± 3.5	21.1 ± 12.9	35.0 ± 2.2	80.6 ± 4.8	20.2 ± 6.1	94.4 ± 33.3	80.2 ± 9.3	339.4 ± 15.2
UTIGSP($\alpha=1e-7$)	6.2 ± 3.5	20.0 ± 11.5	32.5 ± 2.1	75.2 ± 9.9	21.2 ± 4.5	103.0 ± 22.1	78.9 ± 9.2	348.7 ± 12.6
UTIGSP($\alpha=1e-9$)	7.6 ± 3.8	22.3 ± 13.4	33.9 ± 2.0	78.6 ± 6.9	19.5 ± 4.1	94.9 ± 31.9	77.2 ± 7.4	341.8 ± 19.3
DCDI-G	3.4 ± 4.2	6.9 ± 7.5	3.3 ± 1.3	20.4 ± 10.4	21.8 ± 32.1	20.9 ± 12.3	20.1 ± 8.1	104.6 ± 47.1
DCDI-DSF	7.8 ± 7.9	11.8 ± 5.7	3.3 ± 1.2	23.2 ± 9.1	27.4 ± 30.9	49.3 ± 15.7	22.2 ± 10.4	131.0 ± 41.0